Universiteit Leiden
The Netherlands

New statistical methods for analysing resting state functional magnetic resonance imaging to detect localised differences

YueXiang Teo

Thesis advisor:

Prof. Dr. Serge Rombouts, LU-FSW

Dr. Wouter Weeda, LU-FSW

Defended on 18 January, 2026

MASTER THESIS

STATISTICS AND DATA SCIENCE

UNIVERSITEIT LEIDEN

Contents

Abstract

Functional magnetic resonance imaging (fMRI) is a widely used neuroimaging technique used to study brain activity through the blood oxygenation level-dependent (BOLD) signal in the brain. While task-based fMRI is more commonly used to examine neural response to specific stimuli, resting state fMRI (rs-fMRI) of spontaneous brain activity has been garnering more attention in recent years. More popular methods for rs-fMRI seek to identify functional connectivity between brain regions. Although effective at mapping global brain networks, connectivity-based approaches can overlook localised information contained in region-level signals.

In this thesis, we explore alternative analyses that emphasize local and region-specific signal characteristics. We use various statistical measures to characterise the rs-fMRI signal and statistically test their ability to differentiate between patients with cognitive decline and control groups. Specifically, seven statistical measures are examined: mean without cerebrospinal fluid regression, standard deviation (SD), amplitude of low frequency fluctuations (ALFF), fractional ALFF, spectral centroid, spectral variance, and spectral skewness. From our dataset, SD of the BOLD signal seems to be the most informative statistical measure in differentiating patients from controls. Moreover, the SD shows potential for tracking cognitive decline progress. While several other statistical measures show promise in differentiating specific cognitive decline diagnoses, they appear to be less suitable to track decline. These findings suggest that local and region-specific signal characteristics may contain relevant information on local brain function and dysfunction and can complement functional connectivity research to provide more insights into brain function and dysfunction.

1. Introduction

Magnetic resonance imaging (MRI) is a non-invasive imaging technique used to study body anatomy, including brain anatomy, cerebral blood flow, cerebral metabolism, and brain function, the latter using functional magnetic resonance imaging (fMRI). fMRI is an extension of MRI that focuses on the blood oxygenation level-dependent (BOLD) signal in the brain (Ogawa et al., 1990). Through this innovation, fMRI has allowed us to improve understanding of brain activation and subsequently the functioning of the brain.

Despite these advances, there is still much to learn and explore, such as how the brain cells – neurons, operate to produce complex brain functions (Roland, 2023), and how alterations in these functions can lead to different neurological conditions. Traditionally, fMRI measures the change in BOLD signal in response to specific stimuli or tasks. While this approach has yielded meaningful insights, it can be limited by task designs, and neurological conditions of patients. In contrast, resting-state fMRI (rs-fMRI) has emerged as a powerful alternative, focusing on spontaneous fluctuations in the BOLD signal that occur in the absence of explicit tasks.

In this thesis, we aim to explore and compare different statistical measures for analysing resting-state BOLD fluctuations across populations. By characterizing and quantifying differences in resting-state activity, we seek to identify potential measures that distinguish healthy and altered brain states, thereby contributing to a better understanding of region-level analysis and its relevance to neurological conditions

1.1. Functional magnetic resonance imaging (fMRI)

During increasing brain activity, neuronal activation leads to increased energy demand, which is met through increased oxygen consumption, a phenomenon known as neurovascular coupling (Fox & Raichle, 1986; Roy & Sherrington, 1890). This increases the oxygenated blood flow into the brain to meet the demand. Haemoglobin is a protein that binds oxygen to be transported in the red blood cell. As oxygen gets used, the haemoglobin gets deoxygenated, which changes the levels of oxyhaemoglobin (haemoglobin with oxygen) and deoxyhaemoglobin (haemoglobin without oxygen). Deoxyhaemoglobin, having a different magnetic property from oxyhaemoglobin, therefore serves as a contrast agent in MRI, allowing us to use it to measure any fluctuation. This principle underlies the basis for BOLD signal, which allows fMRI to indirectly reflect neural activities through the fluctuations in oxyhaemoglobin and deoxyhaemoglobin levels (Ogawa et al., 1990).

1.2. Task-based fMRI

Typically, fMRI studies investigate brain activities using neural response to a specific task stimulus. This response is then compared to the baseline or 'resting' condition (Bandettini et al., 1992; Joares et al., 2017). This allows researchers to identify brain regions that have a significant change in BOLD signal during task execution, which is often an increase in BOLD signal magnitude. However, task-based fMRI is not without challenges. Task-based fMRI often requires careful planning, to ensure that the results are truly associated with the task (Batouli & Sisakhti, 2020). The task-based activation may include less relevant activation, which can confound interpretation (Fakhri et al., 2013). In addition, altered neurological conditions due to disease or medication may impair task execution (Caulo et al., 2011). These factors can ultimately reduce the reliability of data analysis and the accuracy of conclusions drawn from task-based fMRI experiments.

1.3. Resting state fMRI

An alternative method to study brain activity uses rs-fMRI, which has been gaining more attention. Unlike task-based fMRI, rs-fMRI examines the spontaneous fluctuations in BOLD signal of the subject at 'rest', thereby removing the task requirement. Research has shown that BOLD signal fluctuations occur even in the absence of task and stimuli (Fox and Raichle, 2007). Further research has also shown that most of the energy used in the brain is due to these intrinsic activities rather than task-related activations (Raichle, 2015). Hence, the study of rs-fMRI shows promise to better understand the brain.

The premise of this thesis is that different populations have different rs-fMRI signal due to the different functional architecture, allowing for comparison between them. This is supported by research showing that rs-fMRI have consistent patterns across heathy subjects, indicating reliability and reproducibility of BOLD signals (Damoiseaux et al., 2006). Research has also shown altered rs-fMRI patterns in neurological conditions such as Alzheimer's Disease (AD) (Chavarría-Elizondo et al., 2025). These allow for meaningful comparison between different populations, in which the differences of rs-fMRI can reflect neurological changes associated with disease.

1.4. Functional connectivity

One common approach of analysing rs-fMRI data is to map brain networks by modelling functional connectivity between brain regions. This stems from the idea that brain regions do not work in isolation; rather complex functions such as cognition is a result of network activity between brain regions (McIntosh, 2000). Functional connectivity is typically inferred when two or more brain regions exhibit correlated BOLD signal fluctuations over time. The strength of correlation can be quantified as a functional

connectivity score, usually the correlation coefficient (Poldrack et al., 2011, Chapter 8). This allows for analysis for comparing brain networks and patterns of connectivity such as differentiating resting state functional connectivity networks between controls and patients with AD (De Vos et al., 2017; Wang et al., 2006).

1.5. Research aim

However, the approach using connectivity can overlook information contained in region-level signals, such as direct inference of brain regions (Schöttner Sieler, et al., 2025). Hence, in this paper, we aim to explore, develop and evaluate region-level analyses, which can be used complementary to functional connectivity to provide more insights related to regional spontaneous BOLD signals. We will explore different statistical measures to characterise the regional BOLD signal such as mean, standard deviation, amplitude of low frequency fluctuations (ALFF), and spectral analysis measures. We will compare these measures between groups of populations: control and patients with cognitive decline such as AD, and test if the mean of the measures between populations are significantly different.

2. Methods

2.1. Data

In this thesis, two sets of patients and controls data will be used. The data are fMRI time-series. The data have an initial pre-processing done to prepare for data analysis. The data collection and pre-processing step are completed outside the scope of this thesis.

The first set of data comes from a subset of data used in the analysis done by De Vos et al. (2017). The patients are scanned at the Medical University of Graz and clinically diagnosed with probable AD according to the DSM-IV criteria (Association, 2000b). 10 controls and 10 patients are randomly chosen from the dataset to be used in this thesis. Rs-fMRI scan parameters: 150 volumes with TR = 3000 ms, TE = 30 ms, flip angle = 90°, 40 axial slices, with an isotropic voxel size of 3 mm. This data set will be referred as Graz dataset for this thesis.

The second set of data are collected by Leiden University Medical Center (LUMC) (Drenth et al, 2025). The patients are diagnosed with subjective cognitive impairment (SCI), mild cognitive impairment (MCI), and probable AD or mixed type dementia according to the National Institute of Neurological and Communicative Disorders and Stroke and Alzheimer's Disease and Related Disorders Association (NINCDS-ADRDA) criteria (McKhann et al., 2011). The data consists of 39 controls, 22 SCI, 21 MCI, and 11 AD-related patients. Rs-fMRI scan parameters: 200 volumes with TR = 2200 ms, TE = 30

ms, flip angle = 80°, 38 slices, voxel size 2.75 mm. This dataset will be separated by the patients' diagnosis and be referred as LUMC-SCI, LUMC-MCI, and LUMC-AD when comparing with the LUMC-controls for this thesis.

While BOLD signals can indirectly relate to neural activity via neurovascular coupling, the raw measured fMRI signals can contain various noise and artifacts that can hinder accurate data analysis. Common artefacts include noise from the MRI machine, head motion, slice-acquisition timing differences, and magnetic field inhomogeneities. Hence, a pre-processing step is usually required for more reliable fMRI data analysis (Poldrack et al., 2011, Chapter 3). Pre-processing aims to correct and reduce various noise and artifacts. Pre-processing is also done to align individual scans to a common brain space so that data between subjects are comparable. In this thesis, the data are pre-processed using the FMRIB Software Library (FSL) software (Jenkinson et al., 2011). The functional data is registered onto a MNI152 2mm space (Montreal Neurological Institute). The resulting pre-processed data is a four-dimensional data, shape of 91 x 109 x 91 x 150/200, where the first 3 axis are x, y, z voxels (3-dimension axis for fMRI) in MNI152_2mm space and the last axis is the time series data.

2.1.1. Removing CSF

In this thesis, in addition to the pre-processing done, the data will be further processed by removing the cerebrospinal fluid (CSF) noise. CSF is a body fluid found within the central nervous system that serves many key functions, including support and protection (Saladin, 2012, pp. 394–396), homeostatic regulation (Sakka et al., 2011), and waste removal (Benveniste et al., 2017). Although CSF is essential for the nervous system, it does not contain neuronal tissues that produce meaningful BOLD signals. Instead, the circulation of CSF around the brain can introduce fluctuation noise into the fMRI data. Therefore, CSF-related signals are removed to improve the accuracy of statistical inference of neural activity. In this thesis, to minimize these confounding effects, CSF is scaled and removed via regression. The relevant CSF data are extracted from left and right ventricle, located at (-10, -16, 22) and (12, -16, 22) in MNI space, which is also (50, 55, 47) and (39, 55, 47) in voxel space.

Scaling**:** CSF is scaled to a similar level across participants to ensure the measurements are comparable with each other. The scaled CSF will serve as a consistent baseline for comparison, and any differences in signals would be unrelated individual scale. This is achieved by first calculating the mean value of all CSF regions, dividing by the calculated value, then multiplying by a reference value.

$$x_i'(t) = x_i(t) \cdot \frac{RT}{\sum_{j=1}^{R}\sum_{t=1}^{T} y_{jt}} \cdot C_{Ref} \quad (1)$$

where $x_i(t)$ is a fMRI time series data of voxel $i, j \in$ selected CSF regions, and y_{jt} is the time point data of each fMRI data in CSF region. The selected CSF regions are the 2 CSF

points mentioned above. The reference value chosen in this thesis is 10,000. This ensures that the mean CSF value for any sample is 10,000.

Regression**:** After scaling, a regression is applied to statistically remove CSF-related noise from the data to obtain the BOLD signal. The regression uses the mean CSF time series data from the CSF regions as the covariate. The regression approach is a common and simple method that is available in many fMRI processing software packages (Behzadi et al., 2007).

$$X_i(t) = x_t'(t) - \beta_i \cdot \overline{CSF(t)} \quad (2)$$

where β_i is the regression coefficient of the mean of $CSF(t)$ with respect to the fMRI time series data of each voxel, $x_t'(t)$.

2.1.2. Voxel-level and atlas anatomical region-level analysis

In this thesis, we will be analysing the data at individual voxel-level regions, and atlas anatomical region-level. Voxel refers to the spatial resolution of the fMRI data and represents a three-dimensional unit volume of brain tissues from which the fMRI signal is obtained. Voxel-level analysis treats each voxel as independent spatial unit, using the corresponding fMRI signal to enable more localised statistical inference of brain activity.

Atlas anatomical region-level analysis uses the mean fMRI signal aggregated across all the voxels within a predefined anatomical region. Consequently, each region is represented by a singular mean fMRI signal, which is then use for statistical inference. This allows for a more global region-level inference. For this thesis, two anatomical structural atlases are used for the region-level analysis, which are the cortical and subcortical structural areas from the Harvard-Oxford atlas. The atlases will be referred as Atlas 1 and Atlas 2 respectively. The Harvard Oxford atlas is a common probabilistic atlas aligned to the MNI152 space. Atlas 1 (cortical structural area atlas) contains 48 regions, while the Atlas 2 (subcortical structural area atlas) contains 21 regions (Desikan et al., 2006, Makris et al., 2006). Therefore, Atlas 1 region-level analysis will have a 48 time series data, while the Atlas 2 region-level analysis will have a 21 time series data. The two atlases will also be used as a mask to retain valid voxels for statistical analysis. This ensures that voxel data used in analysis are standardised to a widely used atlas, and voxels outside of brain volume are not included for analysis.

2.2. Statistical measures

Various statistical measures will be applied separately to characterise the time-series data into lower-dimensional data. We will explore if the applied statistical measure can be used to differentiate the control and patient populations. Seven statistical measures will be used, namely mean without CSF regression (MeanNR), standard deviation (SD),

amplitude of low frequency fluctuations (ALFF), fractional ALFF (fALFF), spectral centroid (SpCent), spectral variance (SpVar), and spectral skewness (SpSkew)

2.2.1. Mean with no regression (MeanNR)

The first statistical measure is the time series mean, which is the average of the fMRI signal strength along the time-series. The time series mean uses the fMRI signal without CSF regression. This is to allow for interpretation for brain atrophy. Neurological conditions such as AD have shown to result in brain regions atrophy (Heo et al., 2025; Mouton et al., 1998; Woodworth et al., 2022). CSF volume has shown to be linked to brain atrophy, mostly due to filling the space left due to atrophy (Bendel et al., 2009; De Vis et al., 2015). Hence, fMRI data is not regressed to allow identification of increased CSF volume when compared to normal brain activations.

$$\bar{X}_i = \frac{\sum_{t=1}^{T} X'_{it}}{T} \tag{3}$$

where X'_{it} is the processed fMRI signal of region i with CSF scaling and without CSF regression, t is the index of each timepoints, and T is the total number of timepoints.

2.2.2. Standard deviation (SD)

The standard deviation of the time series data describes the spread of the time series data around the time series mean. Temporal standard deviation describes the temporal variability of the signal and has shown to have differences between different populations (Garrett et al., 2010; Månsson et al., 2021).

$$SD_i = \sqrt{\frac{\sum_{t=1}^{T}(X_{it} - \bar{X}_i)^2}{T-1}} \tag{4}$$

where X_{it} is the BOLD signal of region i, which is the processed data after both CSF scaling and regression of the fMRI signal.

2.2.3. Amplitude of low frequency fluctuations (ALFF) and fALFF

Amplitude of low frequency fluctuations (ALFF) is not a common statistical measure, but one used in rs-fMRI analysis. ALFF is a measure of the amplitude of fMRI signal fluctuations in the low-frequency range (typically 0.01 to 0.08 Hz). The low frequency band is grounded from observations showing that low frequency fluctuations can be correlated to the blood oxygenation or flow (Biswal et al., 1995), while higher frequency contains more contributions from physiological noise such as respiratory and cardiac noise (Cordes et al., 2001). Since, ALFF has shown to be related to altered neurological conditions (Li et al., 2018; Turner et al., 2013; Yu-Feng et al., 2006). A variant of ALFF, fractional ALFF (fALFF), has also been proposed to analyse rs-fMRI (Zou et al., 2008),

also showing promise in differentiating altered neurological conditions such as AD (Yang et al., 2019).

ALFF: ALFF is calculated using frequency spectrum analysis rather than the time series data. The time series data is transformed into the frequency domain using Fourier Transform (FT). FT breaks down the time series into various sinusoidal wave function with different frequency and their corresponding complex coefficient. The amplitude of the frequency can be obtained from the magnitude of the complex coefficient. Fast Fourier Transform (FFT) algorithm computes the discrete form of FT, representing the time series in discrete frequency bins and amplitude. ALFF hence uses the mean amplitude in 0.01 to 0.08 Hz frequency range. The ALFF will be standardised using the global mean ALFF value of each sample, allowing for better comparison between samples.

$$\mathrm{ALFF}_i = \frac{\overline{A_{\iota[LF]}}}{\frac{1}{V}\sum_i \overline{A_{\iota[LF]}}} \tag{5}$$

where $\overline{A_{\iota[LF]}}$ is the mean amplitude value within the low frequency band of the FFT of time series data, and V is the number regions of each sample.

fALFF: fALFF is calculated using the ratio of the sum of low frequency amplitude to the sum of entire frequency amplitude.

$$\mathrm{fALFF}_i = \frac{\sum_{LF} A_{i[LF]}}{\sum_i A_i} \tag{6}$$

where A_i is the amplitude of the frequency bin, and $A_{i[LF]}$ is the amplitude within the low frequency band.

2.2.4. Spectral analysis - SpCent, SpVar, SpSkew

Spectral analysis refers to analysis done in the frequency domain, like ALFF. Spectral analysis characterises the data using its frequency spectrum information. Although spectral analysis are well-established methods in digital signal processing, such as audio processing, their applications in fMRI analysis remain relatively novel. In this thesis, we will explore with three spectral analyses: spectral centroid, spectral variance, and spectral skewness, which can be seen as the first, second, and third moments of spectral analysis.

Spectral centroid (SpCent): Spectral centroid indicates the centre of mass of the frequency spectrum. It describes the frequency at which most of spectral power of the signal concentrate around. The spectral power is proportional to the squared of the spectral amplitude, hence can be used to characterise frequency spectrum of the signal. It is still a novel measure in fMRI, but recent research has demonstrated promise in differentiating the resting-state network between individuals (Ries et al., 2018). We

aim to explore if this measure also applies to region-level analysis. The spectral centroid is calculated from the power spectrum.

$$f_{c\_i} = \frac{\sum_k f_{ik}|A_{ik}|^2}{\sum_k |A_{ik}|^2} \tag{7}$$

where f_c is the frequency centroid, f_{ik} is the frequency bin within the frequency range.

Spectral variance (SpVar): Spectral variance indicates the spread of the frequency around the frequency centroid. It is weighted against the normalised spectral power instead of the number of samples as compared to statistical variance.

$$SV_i = \sum_k (f_k - f_{c_i})^2 \cdot p(k) \tag{8}$$

where $p(k) = \frac{|A_{ik}|^2}{\sum_k |A_{ik}|^2}$ is the normalised spectral power of frequency bin k.

Spectral skewness (SpSkew): Spectral skewness measures the asymmetry of the spectrum around the frequency centroid. It indicates if the spread of power lies towards the left or right of the frequency centroid. A positive skewness indicates more power to the right, hence skewing towards higher frequencies. Negative skewness indicates the opposite towards lower frequencies. Zero skewness indicates symmetry around the frequency centroid.

$$SS_i = \frac{m_3}{\sqrt{m_2}^3} \tag{9}$$

where $m_j = \sum_k (f_k - f_{c_i})^j \cdot p(k)$ is the j-th moment of spectrum.

2.3. Statistical hypothesis testing

Statistical hypothesis testing is a statistical method to determine if the observed data provides sufficient evidence to support a proposed hypothesis about the population. This approach allows researchers to determine whether there are statistically significant differences between the control and interest populations. In this thesis, we will test if the mean per region of the samples from each population is statistically different. Using the mean of the statistical measure of each population, a test statistic is calculated and compared to a theoretical probability distribution. The null hypothesis, H_0, which states that there are no significant differences between the mean, will be rejected if the calculated test-statistics falls within of the rejection region in cumulative probability distribution. The hypothesis is defined: $H_0: \mu_a = \mu_b$ and alternative hypothesis $H_a: \mu_a \neq \mu_b$. This is a two-tailed test; hence the rejection areas are on two ends of the probability distribution. This can be translated to calculating the probability of getting the observed test statistic (p-value) and rejecting if the probability falls below the critical value associated with the rejected region. The critical p-value

used for this thesis is 0.05, hence p-values below 0.05 will be considered to have statistical significance. Welch's *t*-test statistic will be used for the statistical hypothesis testing. While they are usually compared to theoretical probability distributions, this thesis will be using permutation testing to generate the sample null probability distribution.

2.3.1. Welch's *t*-test statistic

Welch's *t*-test statistic is used for univariate statistical hypothesis testing to compare the mean of the statistical measures from the two populations sample (Welch, 1947). It is chosen as it allows for unequal variances and sample size under normality from each sample.

$$t = \frac{\overline{X_1} - \overline{X_2}}{\sqrt{\frac{s_1^2}{n_1} + \frac{s_2^2}{n_2}}} \tag{10}$$

where $\overline{X_i}$ is the sample mean of population i, s_i is the sample standard deviation of population i, and n_i is the number of samples in population i.

For large samples or normally distributed populations, Welch's *t*-test statistic is compared with the Student's *t*-distribution. However, we will use the permutation testing to generate the null probability distribution to minimise the normality assumption required for Student's *t*-distribution.

2.3.2. Permutation Testing

Permutation testing is a non-parametric approach used to assess the statistical significance of a test statistics without relying on any specific probability distribution and their assumptions (Good, 1994). Hence, instead of comparing to theoretical probability distributions, permutation testing generates the empirical null distribution using the observed data. Under the null hypothesis that there are no statistically significant differences between the two populations, the observed samples would be exchangeable between the populations. By permuting the samples between the populations and recalculating the test statistics, the distribution of the test statistics should reflect the probability of getting any test statistic under the null hypothesis.

The observed test-statistics can be compared to the generated null distribution and estimating the probability using the following formula:

$$p = \frac{1 + \sum_{k=1}^{K} \mathbf{1}_A(|T_k| \geq |T_{obs}|)}{1 + K} \tag{11}$$

where K is the number of permutations, T_{obs} is the observed test statistic, T_k is the test statistic of k-th permutation, and $\mathbf{1}_A()$ is the indicator function for $|T_k| \geq |T_{obs}|$. $\mathbf{1}_A() =$

1 if $|T_k| \geq |T_{obs}|$, and $\mathbf{1}_A() = 0$ otherwise. The null hypothesis is rejected if the probability is less than the critical value.

However, since each test statistic has their own null distribution, they are not comparable with each other. On the other hand, the *p*-value are comparable as they describe the probability of obtaining the test statistic given each null distribution. Hence, the *p*-values can be converted to a standard test statistic, standard score Z-value. This is done using the inverse cumulative density function (CDF) of the standard normal distribution of mean $\mu = 0$ and standard deviation $\sigma = 1$.

$$Z = \Phi^{-1}(1 - p) \tag{12}$$

where Φ^{-1} is the inverse CDF of standard normal distribution, $N(0,1)$. This ensures that the z-values are comparable with each other.

2.4. Multiple testing corrections

For fMRI statistical hypothesis testing, multiple testing problems are a major concern (Bennett et al., 2009). This problem is due to the large number of statistical inferences performed using statistical hypothesis testing, which increase the likelihood of false inference purely by chance. This is especially the case for voxel-level inference, where the number of tests can exceed 200,000.

For hypothesis testing, the null hypothesis is rejected if the observed test statistic falls within the rejection region. However, even if the null hypothesis is true, there is still a probability that the observed test statistic falls within the rejection region by pure chance of random variation or noise. The cumulative effect of this false inference becomes more pronounced as the number of tests increases and can potentially lead to spurious findings. In short, even with no true differences, some regions can still show statistically significant differences purely by chance. Therefore, it is necessary to apply multiple testing corrections to adjust the significance threshold or *p*-value to control the overall inference across all tests.

2.4.1. False discovery rate (FDR) correction

False discovery rate (FDR) is the rate of rejecting the null hypothesis when it is true (Benjamini & Hochberg, 1995). In this thesis, it refers to finding statistically significant differences even when there are no true differences between the two populations. FDR correction aims to control the expected proportion of false discoveries among all discoveries. This ensures that the observed statistically significant differences are reliable for interpretation, allowing us to find statistically significance differences while limiting the spurious findings expected by chance.

The most common FDR control approach is the Benjamini–Hochberg (BH) procedure. It adjusts the sorted *p*-value according to the number of tests conducted.

$$p_{(r)}{}^{BH} = \min\left(\frac{m}{r} \cdot p_{(r)}, p_{(r+1)}{}^{BH}\right) \quad (13)$$

where m is the total number of tests, r is the sorted rank of the p-value. A minimum function is included to ensure that the sorted $p_{(r)} < p_{(r+1)}$. The test is rejected if the resulting p-value is less than the critical value associated with rejection. The adjustment can also be translated to adjusting the critical value, the threshold for rejection, leading to lesser false positive. FDR corrections will be applied for both voxel-level and region-level analysis.

Voxel-level analysis**:** For voxel-level analysis, three separate FDR correction procedures will be applied.

1. Whole-brain FDR correction, in which FDR correction procedure is applied across all valid voxels within the brain.
2. Atlas 1-based FDR correction, in which FDR correction procedure is performed separately for each region in Atlas 1, limiting each procedure to voxels contained within the region.
3. Atlas 2-based FDR correction, similar to Atlas 1-based FDR correction but using regions defined by Atlas 2.

The motivation to include Atlas based FDR correction is to increase the power to detect true effect within an anatomical region. While whole-brain FDR correction can control the false positive arising from multiple testing, it can also reduce the true positive as a trade-off. Hence, the power to detect true effect reduces, leading to an overly conservative analysis. Atlas based correction addresses this by limit the number of tests used within each set of correction procedure to each anatomical region, thereby increasing the power to detect significance within each region. This approach is particularly useful when only a few regions show evidence of statistical differences, but the differences are not extreme enough to survive whole-brain FDR correction. In such cases, the regionally consistent effects can be corrected to non-significant using whole-brain FDR correction as there are more tests to be considered. By applying the FDR correction within each anatomical region defined by atlases, significant voxels may remain below the critical value, providing more region-specific interpretation for activation differences. However, this increase in power would lead to an increase in false positive across the whole brain, hence extra caution is required when interpretating the result.

FDR correction at the voxel level includes a cluster threshold. Only clusters of spatially connected significant voxels above the predefined minimum cluster size can then be considered as true significant differences. This approach reduces false positive by ensuring that isolated significant voxels are not interpreted as statistically significant. This is due to brain activations tend to activate in spatially connected clusters rather

than isolated voxels. In this thesis, the minimum cluster size is 10 voxels, translating to an 80mm^3 brain volume.

Atlas anatomical region-level analysis**:** FDR correction will also be applied for each of the atlas anatomical region-level analysis. Hence, Atlas 1 region-level analysis will apply the correction procedure for the 48 data, and Atlas 2 region-level analysis will apply the correction procedure for the 21 data.

2.4.2. Cluster-level correction for voxel-level analysis

A cluster-level correction can be used for voxel-level analysis to reduce the likelihood of false discoveries (Bansal & Peterson, 2018). Voxels activations are expected to occur in spatially connected clusters, hence cluster-level correction seeks to identify the minimum cluster threshold associated with true voxel activations. This can be achieved via permutation testing as mentioned in Section 2.3.2. In contrast to estimating the null distribution of test statistic for each voxel, cluster-level correction estimates the null distribution of maximum cluster size. The largest cluster size of test statistic above the critical test statistic threshold after each permutation is used to build the null distribution. As the samples were permutated, the null distribution should reflect the largest cluster size due to pure chance. From this null distribution, a cluster size threshold can be obtained via the cluster size associated with the critical desired percentile. This ensures the probability of observing a cluster size by chance that is larger than the threshold is small enough to be acceptable. Therefore, using the original test statistic map of the whole brain, only clusters larger than the threshold size are considered significant. This approach is done using the FSL software.

3. Results

This thesis explores different statistical measures for analysing rs-fMRI and statistically tested the mean of the measures between different populations. The alternative hypothesis is defined as $H_a: \mu_a \neq \mu_b$, a two-tailed test. As this study is exploratory in nature, results are limited to the dataset used and should not be generalised as confirmatory findings.

The results section will be organised by the different statistical measures and mainly focus on the statistically significance regions. The voxel-level analysis uses signal data from individual voxels, and the results will be surmised by the proportion of significant voxels across the valid voxels, and voxels outside of brain volume are not included for analysis. Voxel-level analysis results include the whole-brain FDR correction, the two atlases-based FDR corrections, and the whole brain cluster-level correction. The anatomical region-level analysis uses the mean signal data aggregated across all the voxels within a predefined anatomical region, and the results will include the uncorrected and FDR-corrected *p*-value of each region.

3.1. MeanNR

3.1.1. Voxel-level analysis

Table 1 shows the results of MeanNR for the different populations compared to their respective control group. As expected, the proportion of significant voxels decreases after using the different correction methods when compared to the uncorrected *p*-value. The Graz dataset shows a small proportion of statistically significant voxels using MeanNR. For the LUMC dataset, the proportion of statistically significant voxels decreased despite the increase in severity of cognitive decline, with LUMC-AD having less than 0.05 proportion of significant voxels.

Table 2 shows the breakdown of Atlas 1 FDR correction. 37 of the 48 regions of LUMC-SCI have significant voxels within the region, and 27 of them have a proportion of more than 0.5. The number of regions with a proportion of more than 0.5 decrease to 6 and 3 for LUMC-MCI and LUMC-AD respectively. The parahippocampal gyrus (posterior division), lingual gyrus, and temporal occipital fusiform cortex regions from Atlas 1 contain a proportion of more than 0.5 across the three populations.

Table 1: Proportion of significant voxels across all valid voxels using meanNR to characterize fMRI signal

P-value result	Graz	LUMC-SCI	LUMC-MCI	LUMC-AD
Uncorrected P-value	0.061	0.645	0.364	0.222
Whole brain FDR	0	0.587	0.185	0.008
Atlas1 FDR	0	0.297	0.073	0.025
Atlas2 FDR	0.003	0.571	0.171	0.021
Cluster-level	0.001	0.162	0.052	0.016

Note: Graz refers to the hypothesis testing of the patients diagnosed with Alzheimer Disease and control data from subset of data used in the analysis done by De Vos et al. (2017). LUMC-SCI refers to the hypothesis testing of patients diagnosed with subjective cognitive impairment and control from LUMC data (Drenth et al, 2025). MCI refers to the hypothesis testing of patients diagnosed with mild cognitive impairment and control from LUMC data (Drenth et al, 2025). AD refers to the hypothesis testing of patients diagnosed with probable AD or mixed type dementia and control from LUMC data (Drenth et al, 2025). FDR refers to using False Discovery Rate correction procedure on the *p*-value obtained from hypothesis testing. Atlas 1 refers to the cortical structural area atlas from Harvard Oxford atlas. Atlas 2 refers to the subcortical structural area atlas from Harvard Oxford atlas. These varibles will also be used for table 2 – 16.

Table 3 shows the breakdown of Atlas 2 FDR correction. All populations contain regions with statistically significant voxels. LUMC-MCI has the most at 19 regions, followed by LUMC-SCI at 16, LUMC-AD at 9, and Graz at 4. However, the number of regions with proportion more than 0.5 decreases to 8, 11, 4, and 3 respectively, with LUMC-SCI having the most regions, consistent with Atlas 1 FDR correction. The left pallidum, right thalamus, and right pallidum contain a proportion of more than 0.5 across the LUMC populations. Interestingly, the left lateral ventricle shows an increase in proportion of significant voxels with increased severity of cognitive decline, while the right lateral ventricle shows a decreasing trend.

3.1.2. Atlas anatomical region-level analysis

This section shows the results from the atlas anatomical region-level analysis, in which the mean of the time-series data for all the voxels within each anatomical region is used for statistical hypothesis testing. Hence, the number of tests is much lesser than voxel-level analysis.

Table 4 shows the result from Atlas 1. After FDR correction, only LUMC-SCI and LUMC-MCI has regions with *p*-value less than 0.05. LUMC-SCI has 41 regions, while LUMC-MCI has 14 regions.

Table 5 shows the result from Atlas 2. All populations still have regions with *p*-value less than 0.05 after FDR correction. The left pallidum and right pallidum are statistically significant across the LUMC populations.

Table 2: Proportion of significant voxels in each region after Atlas 1 FDR using meanNR to characterize fMRI signal

Atlas1 Region	Graz	LUMC-SCI	LUMC-MCI	LUMC-AD
Frontal Pole	0	0	0	0
Insular Cortex	0	0.953	0.244	0
Superior Frontal Gyrus	0	0.497	0	0
Middle Frontal Gyrus	0	0.700	0	0
Inferior Frontal Gyrus, pars triangularis	0	0.648	0	0
Inferior Frontal Gyrus, pars opercularis	0	0.842	0	0
Precentral Gyrus	0	0.429	0	0
Temporal Pole	0	0	0	0
Superior Temporal Gyrus, anterior division	0	0.775	0	0
Superior Temporal Gyrus, posterior division	0	0.832	0.166	0
Middle Temporal Gyrus, anterior division	0	0.410	0	0
Middle Temporal Gyrus, posterior division	0	0.378	0	0
Middle Temporal Gyrus, temporooccipital part	0	0.773	0	0
Inferior Temporal Gyrus, anterior division	0	0	0	0
Inferior Temporal Gyrus, posterior division	0	0	0	0.025
Inferior Temporal Gyrus, temporooccipital part	0	0.163	0	0
Postcentral Gyrus	0	0.232	0.013	0
Superior Parietal Lobule	0	0	0	0
Supramarginal Gyrus, anterior division	0	0.334	0	0
Supramarginal Gyrus, posterior division	0	0.552	0.118	0
Angular Gyrus	0	0.521	0	0
Lateral Occipital Cortex, superior division	0	0.133	0	0
Lateral Occipital Cortex, inferior division	0	0.621	0.278	0
Intracalcarine Cortex	0	0.657	0.602	0
Frontal Medial Cortex	0	0	0	0
Juxtapositional Lobule Cortex	0	0.525	0.222	0
Subcallosal Cortex	0	0	0	0
Paracingulate Gyrus	0	0.869	0	0
Cingulate Gyrus, anterior division	0	0.885	0.215	0
Cingulate Gyrus, posterior division	0	0.908	0.5	0
Precuneous Cortex	0	0.461	0.345	0
Cuneal Cortex	0	0.521	0.573	0.156
Frontal Orbital Cortex	0	0	0	0
Parahippocampal Gyrus, anterior division	0	0	0	0.093
Parahippocampal Gyrus, posterior division	0	0.700	0.587	0.621
Lingual Gyrus	0	0.897	0.813	0.662
Temporal Fusiform Cortex, anterior division	0	0	0	0
Temporal Fusiform Cortex, posterior division	0	0	0.189	0.449
Temporal Occipital Fusiform Cortex	0	0.952	0.845	0.67
Occipital Fusiform Gyrus	0	0.845	0.454	0.241
Frontal Opercular Cortex	0	0.968	0.137	0
Central Opercular Cortex	0	0.758	0.248	0
Parietal Opercular Cortex	0	0.811	0.132	0
Planum Polare	0	0.900	0.073	0
Heschl's Gyrus (includes H1 and H2)	0	0.806	0	0
Planum Temporale	0	0.935	0.308	0
Supracalcarine Cortex	0	0.529	0.705	0
Occipital Pole	0	0.081	0.047	0

Table 3: Proportion of significant voxels in each region after Atlas 2 FDR using meanNR to characterize fMRI signal

Atlas2 Region	Graz	LUMC-SCI	LUMC-MCI	LUMC-AD
Left Cerebral White Matter	0	0.852	0.307	0
Left Cerebral Cortex	0	0	0.015	0
Left Lateral Ventricle	0	0	0.093	0.137
Left Thalamus	0	0.578	0.48	0.386
Left Caudate	0	0.444	0.088	0
Left Putamen	0	1	0.934	0.04
Left Pallidum	0	1	1	0.708
Brain-Stem	0	0	0.557	0.514
Left Hippocampus	0	0	0	0
Left Amygdala	0.526	0.016	0	0
Left Accumbens	0	0.697	0.764	0
Right Cerebral White Matter	0	0.866	0.423	0.01
Right Cerebral Cortex	0	0	0.076	0
Right Lateral Ventricle	0	0.349	0.044	0
Right Thalamus	0	0.838	0.75	0.684
Right Caudate	0	0.795	0.337	0
Right Putamen	0.073	1	1	0.212
Right Pallidum	0.665	1	1	0.842
Right Hippocampus	0	0.461	0.066	0
Right Amygdala	0.637	0.571	0.478	0
Right Accumbens	0	0.226	0.798	0

Table 4: Uncorrected and corrected *p*-value of each region from the Atlas 1 anatomical region-level analysis using meanNR to characterize fMRI signal

	Graz		LUMC-SCI		LUMC-MCI		LUMC-AD	
Atlas1 Region	P-val	FDR	P-val	FDR	P-Val	FDR	P-Val	FDR
Frontal Pole	0.583	0.718	**0.001**	**0.002**	0.300	0.383	0.102	0.244
Insular Cortex	0.200	0.414	**< 0.001**	**0.002**	0.073	0.129	0.131	0.270
Superior Frontal Gyrus	0.540	0.701	**0.003**	**0.006**	**0.013**	**0.044**	0.079	0.238
Middle Frontal Gyrus	0.735	0.822	**0.001**	**0.002**	**0.037**	0.075	**0.028**	0.168
Inferior Frontal Gyrus, pars triangularis	0.562	0.710	**0.001**	**0.003**	0.699	0.746	0.163	0.290
Inferior Frontal Gyrus, pars opercularis	0.490	0.653	**0.001**	**0.003**	0.489	0.553	0.109	0.248
Precentral Gyrus	0.196	0.414	**0.015**	**0.020**	**0.030**	0.069	0.160	0.290
Temporal Pole	0.224	0.414	**0.022**	**0.026**	0.887	0.887	0.530	0.566
Superior Temporal Gyrus, anterior division	0.181	0.414	**< 0.001**	**0.002**	0.194	0.259	**0.015**	0.122
Superior Temporal Gyrus, posterior division	0.088	0.414	**< 0.001**	**0.001**	**0.025**	0.064	0.100	0.244
Middle Temporal Gyrus, anterior division	0.053	0.414	**0.006**	**0.010**	0.151	0.214	**0.024**	0.163
Middle Temporal Gyrus, posterior division	0.075	0.414	**0.010**	**0.014**	**0.011**	**0.041**	0.158	0.290
Middle Temporal Gyrus, temporooccipital part	0.181	0.414	**< 0.001**	**0.001**	**0.008**	**0.037**	0.326	0.423
Inferior Temporal Gyrus, anterior division	0.696	0.815	**0.004**	**0.007**	0.118	0.177	0.271	0.394
Inferior Temporal Gyrus, posterior division	0.790	0.862	0.259	0.277	**0.025**	0.064	0.353	0.423
Inferior Temporal Gyrus, temporooccipital part	0.936	0.963	**0.035**	**0.041**	**0.019**	0.061	0.195	0.322
Postcentral Gyrus	0.154	0.414	**0.047**	0.051	0.087	0.143	0.312	0.419
Superior Parietal Lobule	0.395	0.574	**0.047**	0.051	0.152	0.214	0.291	0.411
Supramarginal Gyrus, anterior division	0.737	0.822	**0.018**	**0.022**	0.454	0.531	0.427	0.500
Supramarginal Gyrus, posterior division	0.898	0.958	**0.002**	**0.004**	**0.034**	0.074	0.243	0.365
Angular Gyrus	0.973	0.973	**0.005**	**0.009**	**0.025**	0.064	0.237	0.365
Lateral Occipital Cortex, superior division	0.671	0.805	**0.009**	**0.013**	**0.029**	0.069	0.201	0.322
Lateral Occipital Cortex, inferior division	0.157	0.414	**0.001**	**0.002**	**0.002**	**0.019**	0.091	0.243
Intracalcarine Cortex	0.124	0.414	**0.009**	**0.013**	**0.010**	**0.041**	0.091	0.243
Frontal Medial Cortex	0.943	0.963	0.573	0.586	0.886	0.887	0.345	0.423
Juxtapositional Lobule Cortex	0.236	0.414	**0.016**	**0.020**	**0.011**	**0.041**	0.135	0.270
Subcallosal Cortex	0.433	0.593	0.777	0.777	0.841	0.877	0.455	0.508
Paracingulate Gyrus	0.314	0.486	**< 0.001**	**0.002**	0.367	0.452	0.176	0.302
Cingulate Gyrus, anterior division	0.220	0.414	**0.001**	**0.002**	**0.049**	0.095	0.125	0.270
Cingulate Gyrus, posterior division	0.162	0.414	**< 0.001**	**0.002**	**0.006**	**0.033**	**0.038**	0.181
Precuneous Cortex	0.168	0.414	**0.008**	**0.012**	**0.004**	**0.025**	0.058	0.213
Cuneal Cortex	0.234	0.414	**0.007**	**0.012**	**0.004**	**0.025**	0.070	0.223
Frontal Orbital Cortex	0.414	0.584	**0.001**	**0.002**	0.672	0.733	**0.041**	0.181
Parahippocampal Gyrus, anterior division	0.254	0.421	**0.045**	0.051	0.110	0.170	0.057	0.213
Parahippocampal Gyrus, posterior division	0.095	0.414	**< 0.001**	**0.001**	**0.005**	**0.029**	**0.003**	0.058
Lingual Gyrus	0.089	0.414	**< 0.001**	**0.001**	**0.001**	**0.019**	**0.005**	0.058
Temporal Fusiform Cortex, anterior division	0.378	0.567	**0.015**	**0.020**	0.058	0.107	0.928	0.928
Temporal Fusiform Cortex, posterior division	0.232	0.414	**0.001**	**0.002**	**0.037**	0.075	**0.001**	0.058
Temporal Occipital Fusiform Cortex	0.131	0.414	**< 0.001**	**0.001**	**0.001**	**0.019**	**0.004**	0.058
Occipital Fusiform Gyrus	0.135	0.414	**0.001**	**0.002**	**0.001**	**0.019**	**0.012**	0.115
Frontal Opercular Cortex	0.300	0.480	**< 0.001**	**0.001**	0.379	0.454	0.066	0.223
Central Opercular Cortex	0.115	0.414	**0.001**	**0.002**	0.303	0.383	0.507	0.553
Parietal Opercular Cortex	0.085	0.414	**0.001**	**0.002**	0.078	0.133	0.442	0.505
Planum Polare	0.241	0.414	**< 0.001**	**0.002**	0.104	0.166	0.352	0.423
Heschl's Gyrus (includes H1 and H2)	0.153	0.414	**0.002**	**0.004**	0.160	0.220	0.692	0.706
Planum Temporale	0.126	0.414	**< 0.001**	**0.001**	**0.025**	0.064	0.314	0.419
Supracalcarine Cortex	0.130	0.414	**0.011**	**0.015**	**0.003**	**0.025**	**0.034**	0.181
Occipital Pole	0.156	0.414	0.274	0.285	0.496	0.553	0.617	0.644

Table 5: Uncorrected and corrected *p*-value of each region from the Atlas 2 anatomical region-level analysis using meanNR to characterize fMRI signal

	Graz		SCI		MCI		AD	
Atlas2 Regions	P-val	FDR	P-val	FDR	P-Val	FDR	P-Val	FDR
Left Cerebral White Matter	0.390	0.579	**0.002**	**0.004**	**0.024**	**0.043**	0.208	0.313
Left Cerebral Cortex	0.232	0.444	**0.001**	**0.003**	0.057	0.092	0.105	0.201
Left Lateral Ventricle	0.207	0.444	0.125	0.125	0.228	0.281	**0.025**	0.078
Left Thalamus	0.835	0.835	**0.010**	**0.013**	0.138	0.193	0.581	0.642
Left Caudate	0.404	0.579	**0.009**	**0.013**	0.991	0.991	0.466	0.612
Left Putamen	**0.025**	0.105	**0.001**	**0.002**	**0.001**	**0.003**	0.171	0.277
Left Pallidum	0.162	0.444	**0.001**	**0.002**	**< 0.001**	**0.001**	**0.003**	**0.029**
Brain-Stem	0.089	0.312	0.059	0.062	**0.007**	**0.017**	**0.007**	**0.046**
Left Hippocampus	0.232	0.444	**0.024**	**0.028**	0.693	0.728	0.553	0.642
Left Amygdala	**0.004**	**0.046**	**0.029**	**0.032**	0.413	0.481	0.412	0.576
Left Accumbens	0.596	0.659	**0.008**	**0.013**	**0.002**	**0.008**	**0.040**	0.093
Right Cerebral White Matter	0.538	0.659	**< 0.001**	**0.002**	**0.008**	**0.018**	0.170	0.277
Right Cerebral Cortex	0.302	0.529	**0.001**	**0.002**	**0.008**	**0.018**	0.053	0.110
Right Lateral Ventricle	0.414	0.579	**0.001**	**0.002**	0.633	0.700	0.655	0.688
Right Thalamus	0.637	0.669	**0.001**	**0.002**	**< 0.001**	**0.002**	**0.015**	0.078
Right Caudate	0.573	0.659	**0.001**	**0.002**	0.078	0.116	0.940	0.940
Right Putamen	**0.024**	0.105	**< 0.001**	**0.002**	**< 0.001**	**0.001**	**0.026**	0.078
Right Pallidum	**0.011**	0.074	**0.001**	**0.002**	**< 0.001**	**0.001**	**0.001**	**0.021**
Right Hippocampus	0.170	0.444	**0.006**	**0.010**	0.180	0.236	0.571	0.642
Right Amygdala	**0.001**	**0.021**	**0.009**	**0.013**	**0.009**	**0.018**	**0.031**	0.081
Right Accumbens	0.568	0.659	**0.023**	**0.028**	**0.004**	**0.011**	**0.024**	0.078

3.2. SD

3.2.1. Voxel-level analysis

Table 6 shows the results of SD for the different populations. The Graz dataset shows a small proportion of statistically significant voxels using SD, however, applying correction reduces the amount of significant voxel considerably. For the LUMC dataset, the proportion of statistically significant voxels increase as the severity of the cognitive decline diagnosis increases, with AD showing the most statistically significant difference from control.

Table 6: Proportion of significant voxels across all valid voxels using SD to characterize BOLD signal

P-value result	Graz	LUMC-SCI	LUMC-MCI	LUMC-AD
Uncorrected P-value	0.139	0.070	0.202	0.457
Whole brain FDR	0	0	0	0.198
Atlas1 FDR	0.004	0	0.002	0.160
Atlas2 FDR	0	0	0.016	0.199
Cluster-level	0.004	0.003	0.007	0.039

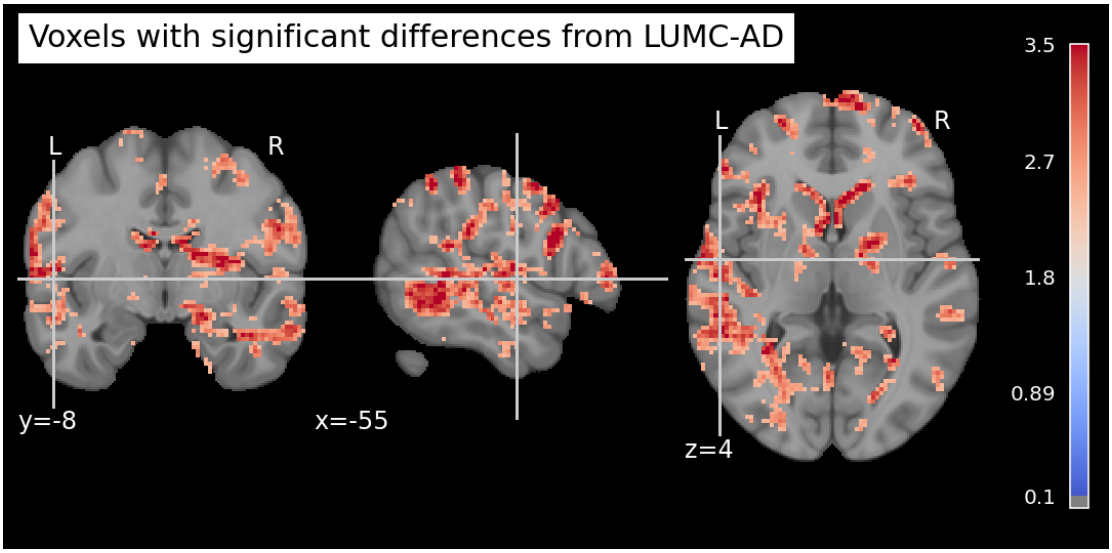

Figure 1: Axial/coronal/sagittal slice view of the Z-score map showing the voxels with significant differences in SD of BOLD signal between patients with probable AD and controls from the LUMC dataset. The Z-score map results are shown after whole-brain FDR correction. Coordinates of slice are at y = -8, x = -55, and z = 4.

Figure 1 shows some axial/coronal/sagittal slices of the brain after whole-brain FDR correction. Only voxels with significant Z-score are coloured in scale of blue to red.

Table 7 shows the breakdown of Atlas 1 FDR correction. LUMC-SCI does not have any region with significant voxels after FDR correction, LUMC-MCI and LUMC-AD have 1 and 34 regions with significant voxels respectively. The number of regions decreased to 0 and 11 for proportion of significant voxels more than 0.5 respectively. Interestingly, parahippocampal gyrus (anterior division) which contains significant voxels in LUMC-MCI does not contain significant voxels in LUMC-AD.

Table 8 shows the result from Atlas 2. Graz and LUMC-SCI does not have any significant voxels after FDR correction, while LUMC-MCI and LUMC-AD have 10 and 17 regions respectively. The number for proportion more than 0.5 decreased to 1 and 4 respectively. While the number of regions for significant voxels increased from LUMC-MCI to LUMC-AD, the proportion significant voxels in each region can decrease. Both left and right of putamen and pallidum are examples in which the proportion of significant voxels decrease from LUMC-MCI to LUMC-AD.

3.2.2. Atlas anatomical region-level analysis

Table 9 shows the result from Atlas 1. After FDR correction, only LUMC-AD has regions with *p*-values less than 0.05.

Table 10 shows the result from Atlas 2. Both LUMC-MCI and LUMC-AD still have regions with *p*-values less than 0.05 after FDR correction. The left caudate and right

lateral ventricle are statistically significant across both populations. The right caudate and right pallidum are statistically significant in LUMC-MCI but not in LUMC-AD.

Table 7: Proportion of significant voxels in each region after Atlas 1 FDR using SD to characterize BOLD signal

Atlas1 Region	Graz	LUMC-SCI	LUMC-MCI	LUMC-AD
Frontal Pole	0	0	0	0.159
Insular Cortex	0	0	0	0
Superior Frontal Gyrus	0	0	0	0.411
Middle Frontal Gyrus	0	0	0	0.218
Inferior Frontal Gyrus, pars triangularis	0	0	0	0.166
Inferior Frontal Gyrus, pars opercularis	0	0	0	0.500
Precentral Gyrus	0	0	0	0.288
Temporal Pole	0	0	0	0.002
Superior Temporal Gyrus, anterior division	0	0	0	0.512
Superior Temporal Gyrus, posterior division	0.056	0	0	0.440
Middle Temporal Gyrus, anterior division	0	0	0	0.393
Middle Temporal Gyrus, posterior division	0	0	0	0.220
Middle Temporal Gyrus, temporooccipital part	0	0	0	0.246
Inferior Temporal Gyrus, anterior division	0	0	0	0
Inferior Temporal Gyrus, posterior division	0	0	0	0
Inferior Temporal Gyrus, temporooccipital part	0	0	0	0.057
Postcentral Gyrus	0	0	0	0.627
Superior Parietal Lobule	0	0	0	0.387
Supramarginal Gyrus, anterior division	0	0	0	0.534
Supramarginal Gyrus, posterior division	0.041	0	0	0.232
Angular Gyrus	0.025	0	0	0.098
Lateral Occipital Cortex, superior division	0	0	0	0.285
Lateral Occipital Cortex, inferior division	0	0	0	0
Intracalcarine Cortex	0	0	0	0
Frontal Medial Cortex	0	0	0	0
Juxtapositional Lobule Cortex	0	0	0	0
Subcallosal Cortex	0	0	0	0.127
Paracingulate Gyrus	0	0	0	0.011
Cingulate Gyrus, anterior division	0	0	0	0
Cingulate Gyrus, posterior division	0.121	0	0	0.504
Precuneous Cortex	0.041	0	0	0.629
Cuneal Cortex	0	0	0	0.544
Frontal Orbital Cortex	0	0	0	0.049
Parahippocampal Gyrus, anterior division	0	0	0.245	0
Parahippocampal Gyrus, posterior division	0.056	0	0	0.618
Lingual Gyrus	0	0	0	0.521
Temporal Fusiform Cortex, anterior division	0	0	0	0
Temporal Fusiform Cortex, posterior division	0	0	0	0.542
Temporal Occipital Fusiform Cortex	0	0	0	0
Occipital Fusiform Gyrus	0	0	0	0
Frontal Opercular Cortex	0	0	0	0.543
Central Opercular Cortex	0	0	0	0.114
Parietal Opercular Cortex	0.008	0	0	0.318
Planum Polare	0	0	0	0.036
Heschl's Gyrus (includes H1 and H2)	0.013	0	0	0.305
Planum Temporale	0	0	0	0.697
Supracalcarine Cortex	0	0	0	0
Occipital Pole	0	0	0	0

Table 8: Proportion of significant voxels in each region after Atlas 2 FDR using SD to characterize BOLD signal

Atlas2 Region	Graz	LUMC-SCI	LUMC-MCI	LUMC-AD
Left Cerebral White Matter	0	0	0.046	0.108
Left Cerebral Cortex	0	0	0	0.249
Left Lateral Ventricle	0	0	0.226	0.75
Left Thalamus	0	0	0	0
Left Caudate	0	0	0.433	0.246
Left Putamen	0	0	0.496	0.038
Left Pallidum	0	0	0.341	0.296
Brain-Stem	0	0	0	0.221
Left Hippocampus	0	0	0.027	0
Left Amygdala	0	0	0	0
Left Accumbens	0	0	0	0
Right Cerebral White Matter	0	0	0	0.126
Right Cerebral Cortex	0	0	0	0.206
Right Lateral Ventricle	0	0	0.314	0.811
Right Thalamus	0	0	0	0.078
Right Caudate	0	0	0.123	0.252
Right Putamen	0	0	0.290	0.221
Right Pallidum	0	0	0.735	0.442
Right Hippocampus	0	0	0	0.104
Right Amygdala	0	0	0	0.536
Right Accumbens	0	0	0	0.643

Table 9: Uncorrected and corrected *p*-value of each region from the Atlas 1 anatomical region-level analysis using SD to characterize BOLD signal

	Graz		LUMC-SCI		LUMC-MCI		LUMC-AD	
Atlas1 Region	P-val	FDR	P-val	FDR	P-Val	FDR	P-Val	FDR
Frontal Pole	0.778	0.849	0.993	0.993	0.653	0.681	0.350	0.358
Insular Cortex	0.108	0.247	0.515	0.993	0.287	0.405	0.124	0.152
Superior Frontal Gyrus	0.244	0.409	0.604	0.993	0.132	0.345	0.053	0.091
Middle Frontal Gyrus	0.833	0.869	0.991	0.993	0.422	0.506	0.327	0.341
Inferior Frontal Gyrus, pars triangularis	0.717	0.820	0.695	0.993	0.640	0.681	0.244	0.273
Inferior Frontal Gyrus, pars opercularis	0.629	0.736	0.978	0.993	0.159	0.345	0.058	0.095
Precentral Gyrus	0.359	0.503	0.577	0.993	0.189	0.345	**0.017**	0.059
Temporal Pole	0.252	0.409	0.317	0.993	0.368	0.465	**0.036**	0.082
Superior Temporal Gyrus, anterior division	**0.014**	0.134	0.780	0.993	0.439	0.510	**0.020**	0.061
Superior Temporal Gyrus, posterior division	**0.006**	0.134	0.829	0.993	0.192	0.345	**0.007**	**0.035**
Middle Temporal Gyrus, anterior division	0.201	0.370	0.249	0.993	0.065	0.240	0.094	0.132
Middle Temporal Gyrus, posterior division	0.263	0.409	0.365	0.993	0.194	0.345	0.208	0.237
Middle Temporal Gyrus, temporooccipital part	**0.046**	0.171	0.873	0.993	0.160	0.345	**0.043**	0.085
Inferior Temporal Gyrus, anterior division	0.959	0.974	0.132	0.993	0.282	0.405	0.106	0.142
Inferior Temporal Gyrus, posterior division	0.443	0.559	0.892	0.993	0.241	0.405	0.116	0.151
Inferior Temporal Gyrus, temporooccipital part	0.309	0.464	0.898	0.993	0.124	0.345	**0.048**	0.086
Postcentral Gyrus	0.068	0.191	0.550	0.993	0.114	0.342	**0.005**	**0.029**
Superior Parietal Lobule	0.437	0.559	0.452	0.993	0.616	0.672	**0.041**	0.085
Supramarginal Gyrus, anterior division	0.414	0.552	0.356	0.993	0.052	0.240	**0.001**	**0.022**
Supramarginal Gyrus, posterior division	**0.022**	0.134	0.393	0.993	0.263	0.405	**0.017**	0.059
Angular Gyrus	**0.006**	0.134	0.751	0.993	0.155	0.345	0.263	0.287
Lateral Occipital Cortex, superior division	**0.040**	0.162	0.408	0.993	0.381	0.469	**0.028**	0.068
Lateral Occipital Cortex, inferior division	0.130	0.271	0.924	0.993	0.059	0.240	**0.045**	0.085
Intracalcarine Cortex	0.096	0.240	0.838	0.993	**0.037**	0.240	0.067	0.104
Frontal Medial Cortex	0.616	0.736	0.054	0.993	0.840	0.840	0.299	0.318
Juxtapositional Lobule Cortex	0.605	0.736	0.842	0.993	0.265	0.405	0.067	0.104
Subcallosal Cortex	0.974	0.974	0.206	0.993	0.447	0.510	**0.015**	0.059
Paracingulate Gyrus	0.774	0.849	0.169	0.993	0.359	0.465	0.106	0.142
Cingulate Gyrus, anterior division	**0.025**	0.134	0.705	0.993	0.367	0.465	0.086	0.125
Cingulate Gyrus, posterior division	**0.013**	0.134	0.901	0.993	0.191	0.345	**0.023**	0.066
Precuneous Cortex	**0.025**	0.134	0.887	0.993	0.167	0.345	**0.011**	0.052
Cuneal Cortex	0.159	0.305	0.830	0.993	0.066	0.240	**0.018**	0.059
Frontal Orbital Cortex	0.827	0.869	0.624	0.993	0.245	0.405	0.127	0.153
Parahippocampal Gyrus, anterior division	0.359	0.503	0.072	0.993	0.053	0.240	0.205	0.237
Parahippocampal Gyrus, posterior division	**0.040**	0.162	0.149	0.993	0.775	0.792	**0.001**	**0.022**
Lingual Gyrus	0.055	0.188	0.939	0.993	**0.050**	0.240	**0.027**	0.068
Temporal Fusiform Cortex, anterior division	0.264	0.409	0.341	0.993	0.068	0.240	0.571	0.571
Temporal Fusiform Cortex, posterior division	0.367	0.503	0.421	0.993	0.075	0.240	**0.001**	**0.022**
Temporal Occipital Fusiform Cortex	0.117	0.254	0.892	0.993	**0.045**	0.240	**0.028**	0.068
Occipital Fusiform Gyrus	**0.040**	0.162	0.907	0.993	**0.033**	0.240	**0.046**	0.085
Frontal Opercular Cortex	0.217	0.386	0.928	0.993	0.067	0.240	**0.018**	0.059
Central Opercular Cortex	0.062	0.191	0.565	0.993	0.069	0.240	**0.003**	**0.026**
Parietal Opercular Cortex	0.144	0.287	0.756	0.993	0.074	0.240	**0.005**	**0.029**
Planum Polare	0.065	0.191	0.863	0.993	0.600	0.669	**0.042**	0.085
Heschl's Gyrus (includes H1 and H2)	**0.013**	0.134	0.775	0.993	0.287	0.405	**0.003**	**0.026**
Planum Temporale	**0.018**	0.134	0.726	0.993	0.194	0.345	**0.002**	**0.022**
Supracalcarine Cortex	0.081	0.216	0.969	0.993	0.074	0.240	0.070	0.104
Occipital Pole	0.100	0.240	0.389	0.993	0.297	0.407	0.123	0.152

Table 10: Uncorrected and corrected *p*-value of each region from the Atlas 2 anatomical region-level analysis using SD to characterize BOLD signal

	Graz		SCI		MCI		AD	
Atlas2 Regions	P-val	FDR	P-val	FDR	P-Val	FDR	P-Val	FDR
Left Cerebral White Matter	0.862	0.952	0.708	0.826	0.087	0.167	0.169	0.197
Left Cerebral Cortex	0.133	0.413	0.500	0.801	0.158	0.204	**0.022**	0.060
Left Lateral Ventricle	0.801	0.952	0.220	0.420	**0.027**	0.097	**< 0.001**	**0.002**
Left Thalamus	0.654	0.952	0.874	0.887	0.175	0.204	0.098	0.171
Left Caudate	0.936	0.952	**0.009**	0.161	**0.002**	**0.017**	**0.010**	**0.041**
Left Putamen	0.092	0.413	0.537	0.801	**0.028**	0.097	0.121	0.182
Left Pallidum	0.947	0.952	0.297	0.520	**0.062**	0.167	0.156	0.192
Brain-Stem	0.244	0.568	0.088	0.287	0.150	0.204	0.232	0.256
Left Hippocampus	0.120	0.413	0.620	0.808	0.125	0.202	**0.005**	**0.036**
Left Amygdala	**0.024**	0.413	0.887	0.887	0.073	0.167	**0.027**	0.063
Left Accumbens	0.847	0.952	0.096	0.287	0.088	0.167	0.128	0.182
Right Cerebral White Matter	0.887	0.952	**0.572**	0.801	0.188	0.208	0.136	0.182
Right Cerebral Cortex	0.124	0.413	0.654	0.808	0.168	0.204	**0.039**	0.081
Right Lateral Ventricle	0.408	0.857	0.136	0.336	**0.001**	**0.010**	**< 0.001**	**0.002**
Right Thalamus	0.559	0.952	0.144	0.336	**0.112**	0.196	0.313	0.329
Right Caudate	0.952	0.952	**0.031**	0.161	**0.001**	**0.010**	0.058	0.111
Right Putamen	0.138	0.413	**0.811**	0.887	**0.065**	0.167	0.375	0.375
Right Pallidum	0.648	0.952	**0.018**	0.161	**0.007**	**0.039**	0.139	0.182
Right Hippocampus	0.066	0.413	**0.029**	0.161	0.550	0.550	**0.023**	0.060
Right Amygdala	0.174	0.458	0.071	0.287	0.295	0.310	**0.020**	0.060
Right Accumbens	0.820	0.952	0.195	0.409	0.171	0.204	**0.009**	**0.041**

3.3. ALFF

3.3.1. Voxel-level analysis

Table 11 shows the results of ALFF for the different populations. All population shows small proportion of significant voxels, which decrease to minuscule proportion after corrections. Only LUMC-SCI and LUMC-AD still have significant voxels after Atlas 1 FDR.

For Atlas 1 FDR correction, LUMC-SCI has a proportion of 0.004 of significant voxels in middle temporal gyrus (posterior division), while LUMC-AD has a proportion of 0.029 of significant voxels in planum temporale. The other populations contain no significant voxels.

Table 11: Proportion of significant voxels across all valid voxels using ALFF to characterize BOLD signal

P-value result	Graz	LUMC-SCI	LUMC-MCI	LUMC-AD
Uncorrected P-value	0.139	0.055	0.058	0.088
Whole brain FDR	0	0	0	0
Atlas1 FDR	0	<0.001	0	<0.001
Atlas2 FDR	0	0	0	0
Cluster-level	0.001	0.001	<0.001	0.001

3.3.2. Atlas anatomical region-level analysis

For both Atlas 1 and Atlas 2 region-level analysis, only a few regions have *p*-value less than 0.05 before correction, and no regions are left after FDR correction. (Refer to Appendix Table A-1 and Table A-2 for detailed breakdown)

3.4. fALFF

3.4.1. Voxel-level analysis

Table 12 shows the results of fALFF for the different populations. While the others have miniscule proportion of significant voxel, LUMC-MCI has larger proportion in comparison. A proportion of significant voxel remains after atlases FDR and cluster-level correction, with LUMC-MIC still having the larger proportion.

For Atlas 1 FDR correction, a significant proportion of voxels are statistically significant in the frontal opercular cortex in LUMC-MCI population, the remaining regions have a small proportion or no significant voxels. A small proportion of Heschl's gyrus (includes H1 and H2) remains for LUMC-AD. The other populations do not contain significant voxels. (Refer to Appendix Table A-3)

For Atlas 2 FDR correction, only left putamen contains significant voxel in the LUMC-MCI population with a proportion of 0.141. The other populations do not contain significant voxels.

Table 12: Proportion of significant voxels across all valid voxels using fALFF to characterize BOLD signal

P-value result	Graz	LUMC-SCI	LUMC-MCI	LUMC-AD
Uncorrected P-value	0.040	0.025	0.163	0.058
Whole brain FDR	0	0	0	0
Atlas1 FDR	0	0	0.004	0.001
Atlas2 FDR	0	0	0.001	0
Cluster-level	<0.001	<0.001	0.005	<0.001

3.4.2. Atlas anatomical region-level analysis

Table 13 shows the result from Atlas 1. After FDR correction, only LUMC-MCI has regions with *p*-value less than 0.05. The number of regions remaining is seven.

For Atlas 2 region-level analysis, all the populations have no region left after FDR correction. (Refer to Appendix Table A-4 for detailed breakdown)

Table 13: Uncorrected and corrected *p*-value of each region from the Atlas 1 anatomical region-level analysis using fALFF to characterize BOLD signal

	Graz		LUMC-SCI		LUMC-MCI		LUMC-AD	
Atlas1 Region	P-val	FDR	P-val	FDR	P-Val	FDR	P-Val	FDR
Frontal Pole	0.868	0.945	0.210	0.971	0.092	0.137	0.324	0.885
Insular Cortex	0.693	0.945	0.757	0.971	**0.006**	**0.048**	0.187	0.885
Superior Frontal Gyrus	0.286	0.945	0.065	0.971	**0.015**	0.078	0.789	0.924
Middle Frontal Gyrus	0.449	0.945	0.260	0.971	0.067	0.128	0.500	0.885
Inferior Frontal Gyrus, pars triangularis	0.897	0.945	0.411	0.971	0.211	0.236	0.292	0.885
Inferior Frontal Gyrus, pars opercularis	0.381	0.945	0.762	0.971	0.099	0.137	0.249	0.885
Precentral Gyrus	0.322	0.945	0.989	0.989	**0.033**	0.099	0.384	0.885
Temporal Pole	0.107	0.945	0.713	0.971	0.170	0.199	0.840	0.932
Superior Temporal Gyrus, anterior division	0.674	0.945	0.802	0.971	0.051	0.111	0.314	0.885
Superior Temporal Gyrus, posterior division	0.592	0.945	0.945	0.971	**0.019**	0.078	0.486	0.885
Middle Temporal Gyrus, anterior division	0.696	0.945	0.141	0.971	**0.037**	0.099	0.777	0.924
Middle Temporal Gyrus, posterior division	0.652	0.945	0.286	0.971	0.098	0.137	0.620	0.893
Middle Temporal Gyrus, temporooccipital part	0.845	0.945	0.870	0.971	0.100	0.137	0.921	0.940
Inferior Temporal Gyrus, anterior division	0.903	0.945	0.137	0.971	**0.050**	0.111	0.387	0.885
Inferior Temporal Gyrus, posterior division	0.639	0.945	0.500	0.971	0.812	0.812	**0.028**	0.681
Inferior Temporal Gyrus, temporooccipital part	0.455	0.945	0.453	0.971	0.168	0.199	0.780	0.924
Postcentral Gyrus	0.173	0.945	0.872	0.971	**0.036**	0.099	0.330	0.885
Superior Parietal Lobule	0.232	0.945	0.885	0.971	0.080	0.137	0.981	0.981
Supramarginal Gyrus, anterior division	0.797	0.945	0.944	0.971	0.151	0.186	0.634	0.893
Supramarginal Gyrus, posterior division	0.553	0.945	0.733	0.971	0.210	0.236	0.870	0.932
Angular Gyrus	0.156	0.945	0.410	0.971	0.118	0.154	0.532	0.885
Lateral Occipital Cortex, superior division	0.140	0.945	0.707	0.971	**0.007**	**0.049**	0.448	0.885
Lateral Occipital Cortex, inferior division	0.431	0.945	0.694	0.971	**0.003**	**0.048**	0.246	0.885
Intracalcarine Cortex	0.446	0.945	0.791	0.971	0.072	0.133	0.389	0.885
Frontal Medial Cortex	0.293	0.945	0.114	0.971	0.122	0.154	0.902	0.940
Juxtapositional Lobule Cortex	0.502	0.945	0.756	0.971	0.077	0.137	0.466	0.885
Subcallosal Cortex	0.933	0.952	0.426	0.971	0.059	0.122	0.836	0.932
Paracingulate Gyrus	0.663	0.945	0.676	0.971	0.066	0.128	0.577	0.893
Cingulate Gyrus, anterior division	0.542	0.945	0.728	0.971	0.103	0.137	0.669	0.893
Cingulate Gyrus, posterior division	0.976	0.976	0.246	0.971	**0.019**	0.078	0.874	0.932
Precuneous Cortex	0.353	0.945	0.254	0.971	**0.006**	**0.048**	0.666	0.893
Cuneal Cortex	0.251	0.945	0.906	0.971	**0.024**	0.082	0.075	0.885
Frontal Orbital Cortex	0.585	0.945	0.828	0.971	0.294	0.313	0.783	0.924
Parahippocampal Gyrus, anterior division	0.504	0.945	0.671	0.971	0.692	0.706	0.407	0.885
Parahippocampal Gyrus, posterior division	0.766	0.945	0.779	0.971	0.286	0.312	0.693	0.899
Lingual Gyrus	0.360	0.945	0.747	0.971	**0.050**	0.111	0.553	0.885
Temporal Fusiform Cortex, anterior division	0.617	0.945	0.900	0.971	0.434	0.453	0.157	0.885
Temporal Fusiform Cortex, posterior division	0.313	0.945	0.951	0.971	**0.019**	0.078	0.327	0.885
Temporal Occipital Fusiform Cortex	0.267	0.945	0.563	0.971	**0.033**	0.099	0.546	0.885
Occipital Fusiform Gyrus	0.077	0.945	0.283	0.971	**0.004**	**0.048**	0.367	0.885
Frontal Opercular Cortex	0.905	0.945	0.566	0.971	**0.001**	**0.048**	0.614	0.893
Central Opercular Cortex	0.821	0.945	0.832	0.971	**0.006**	**0.048**	0.175	0.885
Parietal Opercular Cortex	0.885	0.945	0.860	0.971	**0.021**	0.078	0.100	0.885
Planum Polare	0.607	0.945	0.427	0.971	0.051	0.111	0.102	0.885
Heschl's Gyrus (includes H1 and H2)	0.824	0.945	0.409	0.971	0.098	0.137	**0.013**	0.614
Planum Temporale	0.538	0.945	0.412	0.971	0.092	0.137	0.151	0.885
Supracalcarine Cortex	0.791	0.945	0.916	0.971	0.085	0.137	0.126	0.885
Occipital Pole	0.425	0.945	0.858	0.971	**0.021**	0.078	0.485	0.885

3.5. SpCent

3.5.1. Voxel-level analysis

Table 14 shows the results of SpCent for the different populations. All the populations have small proportion of significant voxel before correction, with LUMC-AD having a very miniscule proportion of significant voxel remaining after Atlas 1 FDR. Cluster-level correction also shows LUMC-AD having the larger proportion of significant voxels.

For Atlas 1 FDR correction, a significant proportion (0.427) of voxels are statistically significant in the cuneal cortex in LUMC-AD population. The other regions do not contain any significant voxels.

3.5.2. Atlas anatomical region-level analysis

For both Atlas 1 and Atlas 2 region-level analysis, no regions are left after FDR correction. (Refer to Appendix Table A-5 and Table A-6 for detailed breakdown)

3.6. SpVar

3.6.1. Voxel-level analysis

Table 15 shows the results of SpVar for the different populations. All the populations have miniscule proportion of significant voxel before correction, with LUMC-SCI having a very miniscule proportion of significant voxel remaining after Atlas 1 FDR correction. Cluster-level correction also shows LUMC-SCI having the larger proportion of significant voxels.

For Atlas 1 FDR correction, while LUMC-SCI still has some significant voxels in insular cortex, the proportion is very small (0.021). The other populations do not contain any significant voxels.

Table 14: Proportion of significant voxels across all valid voxels using SpCent to characterize BOLD signal

P-value result	Graz	LUMC-SCI	LUMC-MCI	LUMC-AD
Uncorrected P-value	0.042	0.083	0.015	0.089
Whole brain FDR	0	0	0	0
Atlas1 FDR	0	0	0	0.003
Atlas2 FDR	0	0	0	0
Cluster-level	<0.001	<0.001	<0.001	0.001

Table 15: Proportion of significant voxels across all valid voxels using SpVar to characterize BOLD signal

P-value result	Graz	LUMC-SCI	LUMC-MCI	LUMC-AD
Uncorrected P-value	0.043	0.056	0.047	0.045
Whole brain FDR	0	0	0	0
Atlas1 FDR	0	<0.001	0	0
Atlas2 FDR	0	0	0	0
Cluster-level	<0.001	0.001	<0.001	<0.001

3.6.2. Atlas anatomical region-level analysis

For both Atlas 1 and Atlas 2 region-level analysis, no regions are left after FDR correction. (Refer to Appendix Table A-7 and Table A-8 for detailed breakdown)

3.7. SpSkew

3.7.1. Voxel-level analysis

Table 16 shows the results of SpSkew for the different populations. All the populations have miniscule proportion of significant voxel before correction, with LUMC-AD having a very miniscule proportion of significant voxel remaining after Atlas 1 FDR. Cluster-level correction also shows LUMC-AD having the larger proportion of significant voxels.

For Atlas 1 FDR correction, only LUMC-AD contains significant voxels. The regions with significant voxels are cuneal cortex (0.650), central opercular cortex (0.034), and postcentral gyrus (0.029). The other populations do not contain significant voxels.

3.7.2. Atlas anatomical region-level analysis

For both Atlas 1 and Atlas 2 region-level analysis, no regions are left after FDR correction. (Refer to Appendix Table A-9 and Table A-10 for detailed breakdown)

Table 16: Proportion of significant voxels across all valid voxels using SpSkew to characterize BOLD signal

P-value result	Graz	LUMC-SCI	LUMC-MCI	LUMC-AD
Uncorrected P-value	0.042	0.114	0.022	0.130
Whole brain FDR	0	0	0	0
Atlas1 FDR	0	0	0	0.005
Atlas2 FDR	0	0	0	0
Cluster-level	<0.001	0.001	<0.001	0.003

4. Discussion

While functional connectivity methods have been the more dominant analytical framework in rs-fMRI research, this thesis shows that region-level measures, at both voxel and anatomical regions, can likewise be used to analyse rs-fMRI and differentiate patients with cognitive decline from healthy controls. Region-level measures help characterise local brain activity and could be used to compliment the network-level insights provided by functional connectivity methods.

The results section shows how the various statistical measures differ between different populations; the discussion section will aim to provide possible interpretations for the observed results. As stated, this study is exploratory in nature, interpretations may not be generalisable to other datasets or populations, and more research should be conducted to confirm these interpretations.

4.1. Graz dataset

Since the Graz dataset with 10 controls and 10 AD patients uses a different control population, the results are not directly comparable with the LUMC data, hence will be separately interpreted. For the Graz dataset, most of the statistical measures do not result in statistical significance when comparing patients with the controls after corrections. The only exception is the Atlas 2-based FDR correction for voxel-level analysis and the Atlas 2 anatomical region-level analysis for MeanNR. For both analysis, left and right amygdala tested significant. However, since MeanNR does not regress the CSF out of the fMRI signal, the differences may not be all attributed to the local brain activity. Further details on interpretating MeanNR are discussed below.

For the remaining statistical measures, while the corrected analysis yields no or very miniscule significant result, SD has the most significant results prior to correction. This means that there are statistical differences between the patient and controls, but the test statistics were not extreme enough to remain significant after correction. This limitation is likely related to the relatively small sample size used. The test statistics are dependent on the sample size, where a larger sample size may increase magnitude of the test statistic, improving the likelihood to remain significant after correction. Therefore, SD shows potential for characterising the BOLD signals to differentiate patients with probable AD with healthy controls with a larger sample size.

4.2. LUMC dataset

The LUMC dataset features different diagnoses of progressive cognitive impairment. In general, cognitive decline should follow from SCI to MCI to AD. This should translate to a progressive trend for the significant differences between patients and control fMRI data, where the fMRI signals from AD patients are more statistically different from

controls than fMRI signal from MCI patients, and MCI are more different when compared to SCI.

4.2.1. SD

From the statistical measures, the SD of the BOLD signal shows a clear progressive trend as the diagnosis severity progresses. The voxel-level analysis has an increasing total proportion of significant voxels, both for uncorrected *p*-values and with the different correction methods. While both LUMC-SCI and LUMC-MCI have no significant voxels left after whole-brain FDR, this might improve with more samples as the test statistics magnitude can increase, and hence lower *p*-value and might remain significant after correction.

Using the less conservative atlas-based FDR correction, the trend of increasing proportion of significant voxels across the whole brain becomes more apparent. However, while this progressive trend is observed for a large majority of the voxels, there are some regions that show a different trend. The parahippocampal gyrus (anterior division) from Atlas 1-based FDR correction only has significant voxels in LUMC-MCI, while both left and right of putamen and pallidum from Atlas 2-based FDR correction shows a decreasing trend. These could indicate regional heterogeneity and that significance differences may not be globally similar across diagnostic groups. A possible explanation might be due to compensatory mechanism of the brain due cognitive decline (Grady et al., 2003; Vorobyov & Bobkova, 2015). However, such mechanism is still speculative and would require further studies. Hence, further research could focus on these regions, and how they affect brain function and dysfunction relating to the different diagnoses.

The anatomical region-level analysis using the mean fMRI signal aggregated across all the voxels within a predefined anatomical region also shows a progressive trend, where the number of significant regions increase with diagnostic severity. In addition, most of the regions observed as significant also exhibit a high proportion of significant voxels from the atlas-based FDR correction of voxel-level analysis. The two analyses provide evidence that the SD of those regions are likely to be more different as cognitive decline progress, allowing for tracking decline through those regions.

However, there are also slight discrepancies between the two analyses. Specifically, some regions can contain a relatively high proportion of significant voxels in the voxel-level analysis but are not significant in the atlas anatomical region-level analysis. One possible explanation is the insufficient statistical power in atlas anatomical region-level analysis, where the test statistics are not sufficiently extreme for significance. This can be improved with more sample size. Another explanation is spatial heterogeneity within the region. If subsets of the voxels within the region exhibit

opposite differences from the controls, the mean calculation could result in cancellation of these effects, reducing the atlas anatomical region-level significance.

Conversely, there are regions where anatomical region-level analysis shows significance but a low/no proportion of significant voxels in the voxel-level analysis after atlas-based FDR correction. A possible explanation is that the statistical differences in each voxel from the region are not very extreme. This could result in loss of significance after the atlas-based FDR correction. On the other hand, the anatomical region-level analysis would aggregate the differences, resulting in significant differences.

Hence, both analyses should be used together to provide a more comprehensive analysis of regional differences associated with cognitive decline. Voxel-level analysis emphasizes high magnitude localised voxels differences, while region-level analysis emphasizes distributed consistent differences.

4.2.2. MeanNR

MeanNR exhibit a trend opposite to what would be expected with increasing diagnostic severity. Since meanNR does not regress out the CSF signal, it may not accurately describe the neuron activations. MeanNR is hypothesized to not only detect statistical differences from BOLD effect, but also differences due to regional brain atrophy, in which patients with brain atrophy would have statistically different signal when compared to control. Accordingly, more severe cognitive decline, which should have more brain atrophy, should produce more statistical differences. However, the observed result contradicts the expectation: LUMC-SCI shows more significant results than LUMC-MCI and LUMC-AD. This finding suggests that the assumption meanNR could be used to detect brain atrophy may not be valid.

A possible explanation is that while the signal is scaled to ensure that the CSF between different samples is comparable, the resulting CSF signals in this thesis might not be directly comparable. This could be a result of a prior scaling done in the pre-processing step conducted outside the scope of this thesis. A prior scaling method which does not depend on making the CSF signal similar could affect the final scaled CSF signal. However, this explanation remains speculative, and hence further research is required to clarify the underlying mechanism and to assess the viability of using MeanNR for rs-fMRI characterisation.

4.2.3. Other statistical measures

The other statistical measures do not show any clear trend as the diagnosis severity progresses. Conversely, some statistical measures only have significant results in a single diagnostic population. Examples include fALFF only having significant regions for atlas region-level analysis in LUMC-MCI, and SpCent only having significant voxels for voxel-level analysis after atlas 1 FDR correction in LUMC-AD. This could be due to the

aforementioned explanation that there might compensatory mechanism of the brain for cognitive decline, hence further research could focus why these characteristics of fMRI signal differs from the controls.

4.2.4. Cluster-level correction

While the other correction methods for the voxel-level analysis may result in no significant voxels left, cluster-level correction still retain some significance. However, the proportion of significant voxels compared to the valid voxels are relatively miniscule. The results are also similar to the other corrections in terms of interpretation. For example, SD has an increasing trend of significant voxels similar to the FDR corrections, or fALFF having a higher proportion of significant voxels in LUMC-MCI, which corresponds to the atlas FDR corrections retaining more significant voxels in LUMC-MCI.

Hence, cluster-level correction is a less conservative correction method compared to the FDR corrections, providing more power to detect significance, while allowing for more false positive results. Due to the similarity in their result interpretation, cluster-level correction could also be used to tackle the multiple testing problem. However, caution is required when using cluster-level correction to interpret regions level effects, especially when clusters span across different regions (Woo et al., 2014).

4.3. Overall Findings

Overall, standard deviation of the BOLD signal seems to be the most informative statistical measure in differentiating patients from controls. It has the most significant results after corrections, while the other statistical measures, except meanNR, have little to no significant result. However, these statistical measures have significance prior to correction, which may indicate that a more extreme test statistic and *p*-value may remain significant after correction. This could be achieved via a larger sample size.

SD also shows potential utility for tracking cognitive decline progress. Nevertheless, extra caution is needed when interpreting analysis relating to anatomical regions. Some of the other statistical measures might be used to differentiate certain diagnosis from control but not used to track decline. Using meanNR to track brain atrophy would not be recommended until further research clarifies the underlying mechanisms.

4.4. Limitation and Future Research

Despite the strengths of this work, certain limitations warrant discussion. Firstly, the two datasets used in this study are relatively small, which may affect the generalisability of the findings. As noted, the test statistics can be affected by the sample size; hence a larger sample size can lead to a different conclusion. Specifically,

a larger sample size could yield larger test-statistics, allowing results to remain significant after multiple testing correction. Consequently, more regions may exhibit significant differences. This sample size limitation also applies for the different sample size for each sample population in LUMC dataset. Increasing the sample size of each population may affect the test statistics and hence the results.

In addition, the CSF-related signals are obtained only from two voxels in this thesis. This is an oversimplification of the CSF-related signals. A more comprehensive method to identify CSF signal could be traced to complete method used as inspiration for the regression of CSF used in this thesis. Behzadi et al. (2007) describe the CompCor method to reduce anatomical noise such as those from white matter and CSF. This involves a more complex model for the fMRI signal but may yield cleaner BOLD signal for further analysis.

Furthermore, this thesis uses Welch's t-test statistics with permutation testing and false discovery rate (FDR) corrections to address the multiple testing problem. These are generally sound and widely accepted choices, but there can be better alternatives depending on different circumstances. The two methods come with their own assumptions and limitations, which can be improved as shown by the many methodological research into these areas. Using different test statistics and correction methods can increase power to detect significant differences.

Another limitation is that this thesis characterises the signal into a single statistical measure for each analysis. This can lead to a loss of information from the signal, as seen by the results, where certain statistical measures are significantly different between controls and specific diagnosis groups, but have no significant result using another measure. For example, LUMC-MCI has no significant result using ALFF, but has significant result using fALFF. Hence, further research can seek to use multiple statistical measure to characterise the signal and use a multi-variate test statistic such as Hotelling's two-sample *t*-squared statistic (See Appendix B).

Lastly, this thesis only shows that there exist statistical differences of statistical measures between different neurological conditions, it does not show inference of neurological conditions using values of these statistical measures. Instead, the results are exploratory in nature and suggest that such statistical measure may serve as informative covariates in future predictive modelling research, improving the accuracy of such classification and prediction of specific disorders, thereby allowing for inference of specific neurological conditions.

5. Acknowledgements

I would like to acknowledge and give my sincere gratitude to my supervisors, Prof. Dr. Serge Rombouts and Dr. Wouter Weeda, for helping me with this thesis. It has been a pleasure working with them on this project.

I am especially thankful to Prof. Dr. Serge Rombouts for his invaluable expertise and insightful advice on the research subject matter. This work could not have been completed without his continuous guidance. I also greatly appreciate his support in providing the necessary data for this thesis.

I am equally grateful to Dr. Wouter Weeda for his knowledge and guidance throughout the project. In addition, I sincerely thank him for his assistance with analyses involving the use of FSL software. These contributions have played a significant role in the successful completion of this thesis.

6. Reference List

- Allen, G., Barnard, H., McColl, R., Hester, A. L., Fields, J. A., Weiner, M. F., Ringe, W. K., Lipton, A. M., Brooker, M., McDonald, E., Rubin, C. D., & Cullum, C. M. (2007). Reduced hippocampal functional connectivity in Alzheimer disease. *Archives of Neurology, 64(10)*, 1482. https://doi.org/10.1001/archneur.64.10.1482
- Association, A. P. (2000b). Diagnostic and Statistical Manual of Mental Disorders, fourth edition, text revision (DSM-IV-TR). In *American Psychiatric Association eBooks*. https://doi.org/10.1176/appi.books.9780890423349
- Bandettini, P. A., Wong, E. C., Hinks, R. S., Tikofsky, R. S., & Hyde, J. S. (1992). Time course EPI of human brain function during task activation. *Magnetic Resonance in Medicine, 25*(2), 390–397. https://doi.org/10.1002/mrm.1910250220
- Bansal, R., & Peterson, B. S. (2018). Cluster-level statistical inference in fMRI datasets: The unexpected behavior of random fields in high dimensions. *Magnetic Resonance Imaging*, *49*, 101–115. https://doi.org/10.1016/j.mri.2018.01.004
- Batouli, S. a. H., & Sisakhti, M. (2020). Some points to consider in a Task-Based FMRI study: A Guideline for beginners. *Frontiers in Biomedical Technologies*. 2020;7(1):52-73. https://doi.org/10.18502/fbt.v7i1.2725
- Behzadi, Y., Restom, K., Liau, J., & Liu, T. T. (2007). A component based noise correction method (CompCor) for BOLD and perfusion based fMRI. *NeuroImage, 37(1)*, 90–101. https://doi.org/10.1016/j.neuroimage.2007.04.042
- Bendel, P., Koivisto, T., Äikiä, M., Niskanen, E., Könönen, M., Hänninen, T., & Vanninen, R. (2009). Atrophic Enlargement of CSF Volume after Subarachnoid Hemorrhage: Correlation with Neuropsychological Outcome. *American Journal of Neuroradiology*, *31*(2), 370–376. https://doi.org/10.3174/ajnr.a1804
- Benjamini, Y., & Hochberg, Y. (1995). Controlling the false discovery Rate: A practical and powerful approach to multiple testing. *Journal of the Royal Statistical Society Series B (Statistical Methodology)*, *57*(1), 289–300. https://doi.org/10.1111/j.2517-6161.1995.tb02031.x
- Bennett, C. M., Wolford, G. L., & Miller, M. B. (2009). The principled control of false positives in neuroimaging. *Social Cognitive and Affective Neuroscience*, *4*(4), 417–422. https://doi.org/10.1093/scan/nsp053
- Benveniste, H., Lee, H., & Volkow, N. D. (2017). The Glymphatic Pathway: Waste Removal from the CNS via Cerebrospinal Fluid Transport. *The Neuroscientist, 23(5),* 454–465. https://doi.org/10.1177/1073858417691030
- Biswal, B., Yetkin, F. Z., Haughton, V. M., & Hyde, J. S. (1995). Functional connectivity in the motor cortex of resting human brain using echo-planar mri. *Magnetic Resonance in Medicine*, *34*(4), 537–541. https://doi.org/10.1002/mrm.1910340409
- Brett, M., Penny, W., & Kiebel, S. (2004). Introduction to random field Theory. In Elsevier eBooks (pp. 867–879). https://doi.org/10.1016/b978-012264841-0/50046-9

- Caulo, M., Esposito, R., Mantini, D., Briganti, C., Sestieri, C., Mattei, P. A., Colosimo, C., Romani, G. L., & Tartaro, A. (2011). Comparison of hypothesis- and a novel hybrid data/hypothesis-driven method of functional MR imaging analysis in patients with brain gliomas. *American Journal of Neuroradiology, 32*(6), 1056–1064. https://doi.org/10.3174/ajnr.A2428
- Chavarría-Elizondo, P., Maturana-Quijada, P., Martínez-Zalacaín, I., Del Cerro, I., Juaneda-Seguí, A., Guinea-Izquierdo, A., Gascón-Bayarri, J., Reñé-Ramírez, R., Urretavizcaya, M., Ferrer, I., Menchón, J. M., Soria, V., & Soriano-Mas, C. (2025). Altered resting-state functional connectivity in individuals at risk for Alzheimer's disease: a longitudinal study. *International Journal of Clinical and Health Psychology*, *25*(2), 100588. https://doi.org/10.1016/j.ijchp.2025.100588
- Cordes, D., Haughton, V. M., Arfanakis, K., Carew, J. D., Turski, P. A., Moritz, C. H., Quigley, M. A., & Meyerand, M. E. (2001). Frequencies contributing to functional connectivity in the cerebral cortex in "resting-state" data. *American Journal of Neuroradiology*, *22*(7), 1326–1333. http://www.ajnr.org/content/22/7/1326.full.pdf
- Damoiseaux, J. S., Rombouts, S. A. R. B., Barkhof, F., Scheltens, P., Stam, C. J., Smith, S. M., & Beckmann, C. F. (2006). Consistent resting-state networks across healthy subjects. *Proceedings of the National Academy of Sciences, 103*(37), 13848–13853. https://doi.org/10.1073/pnas.0601417103
- Desikan, R. S., Ségonne, F., Fischl, B., Quinn, B. T., Dickerson, B. C., Blacker, D., Buckner, R. L., Dale, A. M., Maguire, R. P., Hyman, B. T., Albert, M. S., & Killiany, R. J. (2006). An automated labeling system for subdividing the human cerebral cortex on MRI scans into gyral based regions of interest. *NeuroImage, 31*(3), 968–980. https://doi.org/10.1016/j.neuroimage.2006.01.021
- De Vis, J. B., Zwanenburg, J. J., Van Der Kleij, L. A., Spijkerman, J. M., Biessels, G. J., Hendrikse, J., & Petersen, E. T. (2015). Cerebrospinal fluid volumetric MRI mapping as a simple measurement for evaluating brain atrophy. *European Radiology*, *26*(5), 1254–1262. https://doi.org/10.1007/s00330-015-3932-8
- De Vos, F., Koini, M., Schouten, T. M., Seiler, S., van der Grond, J., Lechner, A., Schmidt, R., de Rooij, M., & Rombouts, S. A. R. B. (2017). A comprehensive analysis of resting state fMRI measures to classify individual patients with Alzheimer's disease. *NeuroImage, 163*, 171–183. https://doi.org/10.1016/j.neuroimage.2017.11.025
- Drenth, N., van Dijk, S. E., Hafkemeijer, A., Rombouts, S. A. R. B., van der Grond, J., & van Rooden, S. (2025). *Early cerebral amyloid angiopathy related pathology is not associated with functional brain organization*. [Unpublished manuscript]. Department of Radiology, Leiden University Medical Center.
- Fakhri, M., Oghabian, M. A., Vedaei, F., Zandieh, A., Masoom, N., Sharifi, G., Ghodsi, M., & Firouznia, K. (2013). Atypical language lateralization: an fMRI study in patients with cerebral lesions. Functional Neurology, 28(1), 55–61. https://pubmed.ncbi.nlm.nih.gov/23731916/

- Fox, M. D., & Raichle, M. E. (2007). Spontaneous fluctuations in brain activity observed with functional magnetic resonance imaging. *Nature Reviews. Neuroscience*, *8*(9), 700–711. https://doi.org/10.1038/nrn2201
- Friston, K. J., Worsley, K. J., Frackowiak, R. S. J., Mazziotta, J. C., & Evans, A. C. (1994). Assessing the significance of focal activations using their spatial extent. *Human Brain Mapping*, *1*(3), 210–220. https://doi.org/10.1002/hbm.460010306
- Garrett, D. D., Kovacevic, N., McIntosh, A. R., & Grady, C. L. (2010). Blood Oxygen Level-Dependent Signal Variability Is More than Just Noise. *Journal of Neuroscience*, *30*(14), 4914–4921. https://doi.org/10.1523/jneurosci.5166-09.2010
- Good, P. (1994). Permutation tests. In *Springer series in statistics*. https://doi.org/10.1007/978-1-4757-2346-5
- Grady, C. L., McIntosh, A. R., Beig, S., Keightley, M. L., Burian, H., & Black, S. E. (2003). Evidence from Functional Neuroimaging of a Compensatory Prefrontal Network in Alzheimer's Disease. *Journal of Neuroscience*, *23*(3), 986–993. https://doi.org/10.1523/jneurosci.23-03-00986.2003
- Heo, D., Kim, M., Lee, Y., Kim, S., Kim, Y. S., Sung, W., & Kim, H. (2025). Unravelling the interplay: brain regional atrophy and neuropsychological function in early Alzheimer's disease. *Frontiers in Aging Neuroscience*, *17*, 1508849. https://doi.org/10.3389/fnagi.2025.1508849
- Hotelling, H. (1931). The generalization of student's ratio. *The Annals of Mathematical Statistics*, *2*(3), 360–378. https://doi.org/10.1214/aoms/1177732979
- Jenkinson, M., Beckmann, C. F., Behrens, T. E., Woolrich, M. W., & Smith, S. M. (2011). FSL. *NeuroImage*, *62*(2), 782–790. https://doi.org/10.1016/j.neuroimage.2011.09.015
- Li, G., Rossbach, K., Jiang, W., & Du, Y. (2018). Resting-state brain activity in Chinese boys with low functioning autism spectrum disorder. *Annals of General Psychiatry, 17*(1). https://doi.org/10.1186/s12991-018-0217-z
- Makris, N., Goldstein, J. M., Kennedy, D., Hodge, S. M., Caviness, V. S., Faraone, S. V., Tsuang, M. T., & Seidman, L. J. (2006). Decreased volume of left and total anterior insular lobule in schizophrenia. *Schizophrenia Research, 83(2–3)*, 155–171. https://doi.org/10.1016/j.schres.2005.11.020
- Månsson, K. N., Waschke, L., Manzouri, A., Furmark, T., Fischer, H., & Garrett, D. D. (2021). Moment-to-Moment brain signal variability reliably predicts psychiatric treatment outcome. *Biological Psychiatry*, *91*(7), 658–666. https://doi.org/10.1016/j.biopsych.2021.09.026
- McIntosh, A. (2000). Towards a network theory of cognition. *Neural Networks, 13*(8–9), 861–870. https://doi.org/10.1016/s0893-6080(00)00059-9
- McKhann, G. M., Knopman, D. S., Chertkow, H., Hyman, B. T., Jack, C. R., Kawas, C. H., Klunk, W. E., Koroshetz, W. J., Manly, J. J., Mayeux, R., Mohs, R. C., Morris, J. C., Rossor, M. N., Scheltens, P., Carrillo, M. C., Thies, B., Weintraub, S., & Phelps, C. H. (2011). The diagnosis of dementia due to Alzheimer's disease: Recommendations from the National

Institute on Aging-Alzheimer's Association workgroups on diagnostic guidelines for Alzheimer's disease. *Alzheimer S & Dementia*, *7*(3), 263–269. https://doi.org/10.1016/j.jalz.2011.03.005

- Mouton, P. R., Martin, L. J., Calhoun, M. E., Forno, G. D., & Price, D. L. (1998). Cognitive decline strongly correlates with cortical atrophy in Alzheimer's dementia. *Neurobiology of Aging*, *19*(5), 371–377. https://doi.org/10.1016/s0197-4580(98)00080-3
- Ogawa, S., Lee, T. M., Kay, A. R., & Tank, D. W. (1990). Brain magnetic resonance imaging with contrast dependent on blood oxygenation. *Proceedings of the National Academy of Sciences of the United States of America, 87*(24), 9868–9872. https://doi.org/10.1073/pnas.87.24.9868
- Poldrack, R. A., Mumford, J. A., & Nichols, T. E. (2011). *Handbook of Functional MRI Data Analysis*. https://doi.org/10.1017/cbo9780511895029
- Raichle, M. E. (2015). The restless brain: how intrinsic activity organizes brain function. *Philosophical Transactions of the Royal Society B Biological Sciences*, *370*(1668), 20140172. https://doi.org/10.1098/rstb.2014.0172
- Ries, A., Chang, C., Glim, S., Meng, C., Sorg, C., & Wohlschläger, A. (2018). Grading of Frequency Spectral Centroid Across Resting-State Networks. *Frontiers in Human Neuroscience*, *12*. https://doi.org/10.3389/fnhum.2018.00436
- Roland, P. E. (2023). How far neuroscience is from understanding brains. *Frontiers in Systems Neuroscience, 17*. https://doi.org/10.3389/fnsys.2023.1147896
- Sakka, L., Coll, G., & Chazal, J. (2011). Anatomy and physiology of cerebrospinal fluid. *European Annals of Otorhinolaryngology Head and Neck Diseases, 128(6)*, 309–316. https://doi.org/10.1016/j.anorl.2011.03.002
- Saladin, K. S. (2012). *Anatomy & physiology: The unity of form and function* (6th ed.). McGraw-Hill.
- Turner, J. A., Damaraju, E., M, V. E. T. G., Mathalon, D. H., Ford, J. M., Voyvodic, J., Mueller, B. A., Belger, A., Bustillo, J., McEwen, S., Potkin, S. G., & Calhoun, V. D. (2013). A multi-site resting state fMRI study on the amplitude of low frequency fluctuations in schizophrenia. *Frontiers in Neuroscience, 7*. https://doi.org/10.3389/fnins.2013.00137
- Vorobyov, V., & Bobkova, N. (2015). The brain compensatory mechanisms and Alzheimer's disease progression: a new protective strategy. *Neural Regeneration Research*, *10*(5), 696. https://doi.org/10.4103/1673-5374.156954
- Wang, L., Zang, Y., He, Y., Liang, M., Zhang, X., Tian, L., Wu, T., Jiang, T., & Li, K. (2006). Changes in hippocampal connectivity in the early stages of Alzheimer's disease: Evidence from resting state fMRI. *NeuroImage, 31(2),* 496–504. https://doi.org/10.1016/j.neuroimage.2005.12.033
- Welch, B. L. (1947). The Generalization of `Student's' Problem when Several Different Population Variances are Involved. *Biometrika*, *34*(1/2), 28. https://doi.org/10.2307/2332510

- Woo, C., Krishnan, A., & Wager, T. D. (2014). Cluster-extent based thresholding in fMRI analyses: Pitfalls and recommendations. *NeuroImage*, *91*, 412–419. https://doi.org/10.1016/j.neuroimage.2013.12.058
- Woodworth, D. C., Sheikh-Bahaei, N., Scambray, K. A., Phelan, M. J., Perez-Rosendahl, M., Corrada, M. M., Kawas, C. H., & Sajjadi, S. A. (2022). Dementia is associated with medial temporal atrophy even after accounting for neuropathologies. *Brain Communications*, *4*(2), fcac052. https://doi.org/10.1093/braincomms/fcac052
- Yang, L., Yan, Y., Li, Y., Hu, X., Lu, J., Chan, P., Yan, T., & Han, Y. (2019). Frequency-dependent changes in fractional amplitude of low-frequency oscillations in Alzheimer's disease: a resting-state fMRI study. *Brain Imaging and Behavior*, *14*(6), 2187–2201. https://doi.org/10.1007/s11682-019-00169-6
- Yu-Feng, Z., Yong, H., Chao-Zhe, Z., Qing-Jiu, C., Man-Qiu, S., Meng, L., Li-Xia, T., Tian-Zi, J., & Yu-Feng, W. (2006). Altered baseline brain activity in children with ADHD revealed by resting-state functional MRI. *Brain and Development, 29(2),* 83–91. https://doi.org/10.1016/j.braindev.2006.07.002
- Zou, Q., Zhu, C., Yang, Y., Zuo, X., Long, X., Cao, Q., Wang, Y., & Zang, Y. (2008). An improved approach to detection of amplitude of low-frequency fluctuation (ALFF) for resting-state fMRI: Fractional ALFF. *Journal of Neuroscience Methods*, *172*(1), 137–141. https://doi.org/10.1016/j.jneumeth.2008.04.012

7. Appendix

Table A-1: Uncorrected and corrected *p*-value of each region from the Atlas 1 anatomical region-level analysis using ALFF to characterize BOLD signal

	Graz		LUMC-SCI		LUMC-MCI		LUMC-AD	
Atlas1 Region	P-val	FDR	P-val	FDR	P-Val	FDR	P-Val	FDR
Frontal Pole	**0.034**	0.376	0.621	0.941	0.139	0.938	**0.014**	0.336
Insular Cortex	0.708	0.829	0.266	0.642	0.678	0.938	0.487	0.754
Superior Frontal Gyrus	**0.004**	0.125	0.057	0.466	0.860	0.938	0.717	0.835
Middle Frontal Gyrus	0.232	0.694	0.616	0.941	0.370	0.938	0.115	0.686
Inferior Frontal Gyrus, pars triangularis	**0.005**	0.125	0.384	0.802	0.093	0.938	0.129	0.686
Inferior Frontal Gyrus, pars opercularis	0.258	0.694	0.865	0.959	0.705	0.938	0.256	0.723
Precentral Gyrus	0.893	0.912	0.293	0.669	0.618	0.938	0.400	0.754
Temporal Pole	0.641	0.796	0.087	0.466	0.360	0.938	0.634	0.801
Superior Temporal Gyrus, anterior division	0.521	0.715	0.838	0.959	0.538	0.938	0.752	0.839
Superior Temporal Gyrus, posterior division	**0.023**	0.374	0.971	0.971	0.855	0.938	0.157	0.686
Middle Temporal Gyrus, anterior division	0.787	0.860	**0.024**	0.466	0.747	0.938	0.886	0.905
Middle Temporal Gyrus, posterior division	0.790	0.860	0.067	0.466	0.814	0.938	0.343	0.754
Middle Temporal Gyrus, temporooccipital part	0.396	0.694	0.627	0.941	0.602	0.938	0.381	0.754
Inferior Temporal Gyrus, anterior division	0.376	0.694	0.068	0.466	0.663	0.938	0.369	0.754
Inferior Temporal Gyrus, posterior division	0.383	0.694	0.564	0.941	0.453	0.938	0.209	0.723
Inferior Temporal Gyrus, temporooccipital part	0.634	0.796	0.484	0.866	0.979	0.994	0.486	0.754
Postcentral Gyrus	0.170	0.694	0.241	0.641	0.521	0.938	0.073	0.686
Superior Parietal Lobule	0.647	0.796	0.100	0.478	0.187	0.938	0.545	0.781
Supramarginal Gyrus, anterior division	0.102	0.621	0.351	0.767	0.844	0.938	0.627	0.801
Supramarginal Gyrus, posterior division	0.619	0.796	0.487	0.866	0.628	0.938	0.872	0.905
Angular Gyrus	0.510	0.715	0.962	0.971	0.631	0.938	0.548	0.781
Lateral Occipital Cortex, superior division	0.806	0.860	**0.049**	0.466	0.427	0.938	0.847	0.903
Lateral Occipital Cortex, inferior division	0.384	0.694	0.842	0.959	0.121	0.938	0.478	0.754
Intracalcarine Cortex	0.345	0.694	0.853	0.959	0.300	0.938	0.690	0.835
Frontal Medial Cortex	0.116	0.621	0.051	0.466	0.353	0.938	0.303	0.736
Juxtapositional Lobule Cortex	0.050	0.402	0.599	0.941	0.759	0.938	0.788	0.859
Subcallosal Cortex	0.428	0.707	0.146	0.583	0.386	0.938	0.411	0.754
Paracingulate Gyrus	0.174	0.694	0.082	0.466	0.527	0.938	0.226	0.723
Cingulate Gyrus, anterior division	0.345	0.694	0.741	0.959	0.467	0.938	0.292	0.736
Cingulate Gyrus, posterior division	0.322	0.694	0.964	0.971	0.414	0.938	0.464	0.754
Precuneous Cortex	0.452	0.707	0.718	0.959	0.620	0.938	0.604	0.801
Cuneal Cortex	0.666	0.800	0.684	0.959	0.195	0.938	0.056	0.677
Frontal Orbital Cortex	0.196	0.694	0.734	0.959	0.295	0.938	**0.047**	0.677
Parahippocampal Gyrus, anterior division	0.968	0.968	0.084	0.466	0.923	0.983	0.476	0.754
Parahippocampal Gyrus, posterior division	0.279	0.694	0.130	0.568	0.322	0.938	0.231	0.723
Lingual Gyrus	0.111	0.621	0.924	0.971	0.280	0.938	0.254	0.723
Temporal Fusiform Cortex, anterior division	0.864	0.902	0.414	0.828	0.942	0.983	0.307	0.736
Temporal Fusiform Cortex, posterior division	0.762	0.860	0.176	0.600	0.782	0.938	0.246	0.723
Temporal Occipital Fusiform Cortex	0.404	0.694	0.794	0.959	0.309	0.938	0.553	0.781
Occipital Fusiform Gyrus	**0.039**	0.376	0.779	0.959	0.089	0.938	0.603	0.801
Frontal Opercular Cortex	0.397	0.694	0.879	0.959	0.082	0.938	0.460	0.754
Central Opercular Cortex	0.484	0.715	0.211	0.600	0.237	0.938	0.143	0.686
Parietal Opercular Cortex	0.456	0.707	0.453	0.866	0.354	0.938	0.155	0.686
Planum Polare	0.497	0.715	0.268	0.642	0.474	0.938	0.993	0.993
Heschl's Gyrus (includes H1 and H2)	0.260	0.694	0.185	0.600	0.710	0.938	0.109	0.686
Planum Temporale	0.179	0.694	0.213	0.600	0.844	0.938	**0.005**	0.230
Supracalcarine Cortex	0.405	0.694	0.862	0.959	0.544	0.938	0.731	0.835
Occipital Pole	0.281	0.694	0.201	0.600	0.994	0.994	0.714	0.835

Table A-2: Uncorrected and corrected *p*-value of each region from the Atlas 2 anatomical region-level analysis using ALFF to characterize BOLD signal

	Graz		SCI		MCI		AD	
Atlas2 Regions	P-val	FDR	P-val	FDR	P-Val	FDR	P-Val	FDR
Left Cerebral White Matter	0.940	0.993	0.156	0.401	0.686	0.996	0.871	0.871
Left Cerebral Cortex	0.377	0.659	0.100	0.401	0.826	0.996	0.346	0.683
Left Lateral Ventricle	0.948	0.993	0.745	0.869	0.535	0.996	0.143	0.683
Left Thalamus	0.068	0.343	0.141	0.401	0.433	0.996	0.585	0.683
Left Caudate	0.993	0.993	**0.020**	0.214	0.053	0.842	0.559	0.683
Left Putamen	0.964	0.993	0.574	0.709	0.582	0.996	0.238	0.683
Left Pallidum	0.204	0.536	0.846	0.888	0.878	0.996	0.176	0.683
Brain-Stem	0.140	0.421	0.210	0.401	0.950	0.996	0.389	0.683
Left Hippocampus	0.082	0.343	0.378	0.566	0.977	0.996	**0.036**	0.683
Left Amygdala	**0.010**	0.202	0.186	0.401	0.996	0.996	0.425	0.683
Left Accumbens	0.336	0.659	0.247	0.420	0.933	0.996	0.554	0.683
Right Cerebral White Matter	0.806	0.993	0.138	0.401	0.861	0.996	0.621	0.686
Right Cerebral Cortex	0.269	0.627	0.260	0.420	0.860	0.996	0.387	0.683
Right Lateral Ventricle	**0.049**	0.340	0.995	0.995	0.080	0.842	0.274	0.683
Right Thalamus	**0.021**	0.223	0.516	0.709	0.908	0.996	0.742	0.780
Right Caudate	0.919	0.993	0.201	0.401	0.277	0.996	0.571	0.683
Right Putamen	0.890	0.993	0.101	0.401	0.970	0.996	0.132	0.683
Right Pallidum	0.136	0.421	0.194	0.401	0.511	0.996	0.527	0.683
Right Hippocampus	0.361	0.659	**0.017**	0.214	0.521	0.996	0.120	0.683
Right Amygdala	0.841	0.993	0.572	0.709	0.479	0.996	0.544	0.683
Right Accumbens	0.924	0.993	0.822	0.888	0.362	0.996	0.500	0.683

Table A-3: Proportion of significant voxels in each region after Atlas 1 FDR using fALFF to characterize BOLD signal

Atlas1 Region	Graz	LUMC-SCI	LUMC-MCI	LUMC-AD
Frontal Pole	0	0	0	0
Insular Cortex	0	0	0	0
Superior Frontal Gyrus	0	0	0	0
Middle Frontal Gyrus	0	0	0	0
Inferior Frontal Gyrus, pars triangularis	0	0	0	0
Inferior Frontal Gyrus, pars opercularis	0	0	0	0
Precentral Gyrus	0	0	0	0
Temporal Pole	0	0	0	0
Superior Temporal Gyrus, anterior division	0	0	0	0
Superior Temporal Gyrus, posterior division	0	0	0.020	0
Middle Temporal Gyrus, anterior division	0	0	0	0
Middle Temporal Gyrus, posterior division	0	0	0.006	0
Middle Temporal Gyrus, temporooccipital part	0	0	0	0
Inferior Temporal Gyrus, anterior division	0	0	0	0
Inferior Temporal Gyrus, posterior division	0	0	0	0
Inferior Temporal Gyrus, temporooccipital part	0	0	0	0
Postcentral Gyrus	0	0	0	0
Superior Parietal Lobule	0	0	0	0
Supramarginal Gyrus, anterior division	0	0	0	0
Supramarginal Gyrus, posterior division	0	0	0	0
Angular Gyrus	0	0	0	0
Lateral Occipital Cortex, superior division	0	0	0	0
Lateral Occipital Cortex, inferior division	0	0	0	0
Intracalcarine Cortex	0	0	0	0
Frontal Medial Cortex	0	0	0	0
Juxtapositional Lobule Cortex	0	0	0	0
Subcallosal Cortex	0	0	0	0
Paracingulate Gyrus	0	0	0	0
Cingulate Gyrus, anterior division	0	0	0	0
Cingulate Gyrus, posterior division	0	0	0.034	0
Precuneous Cortex	0	0	0.081	0
Cuneal Cortex	0	0	0	0
Frontal Orbital Cortex	0	0	0	0
Parahippocampal Gyrus, anterior division	0	0	0	0
Parahippocampal Gyrus, posterior division	0	0	0	0
Lingual Gyrus	0	0	0	0
Temporal Fusiform Cortex, anterior division	0	0	0	0
Temporal Fusiform Cortex, posterior division	0	0	0	0
Temporal Occipital Fusiform Cortex	0	0	0	0
Occipital Fusiform Gyrus	0	0	0	0
Frontal Opercular Cortex	0	0	0.543	0
Central Opercular Cortex	0	0	0	0.040
Parietal Opercular Cortex	0	0	0	0
Planum Polare	0	0	0	0
Heschl's Gyrus (includes H1 and H2)	0	0	0	0.157
Planum Temporale	0	0	0	0
Supracalcarine Cortex	0	0	0	0
Occipital Pole	0	0	0	0

Table A-4: Uncorrected and corrected *p*-value of each region from the Atlas 2 anatomical region-level analysis using fALFF to characterize BOLD signal

	Graz		SCI		MCI		AD	
Atlas2 Regions	P-val	FDR	P-val	FDR	P-Val	FDR	P-Val	FDR
Left Cerebral White Matter	0.335	0.735	0.846	0.968	0.059	0.197	0.842	0.930
Left Cerebral Cortex	0.325	0.735	0.648	0.968	**0.029**	0.197	0.934	0.981
Left Lateral Ventricle	0.748	0.832	0.571	0.968	0.669	0.781	0.273	0.823
Left Thalamus	0.753	0.832	0.793	0.968	0.332	0.537	0.988	0.988
Left Caudate	0.913	0.913	0.395	0.968	0.214	0.450	0.384	0.823
Left Putamen	0.873	0.913	0.503	0.968	0.055	0.197	0.523	0.823
Left Pallidum	0.420	0.735	0.272	0.968	0.209	0.450	0.377	0.823
Brain-Stem	0.089	0.735	0.968	0.968	0.908	0.941	0.418	0.823
Left Hippocampus	0.208	0.735	0.755	0.968	0.055	0.197	0.135	0.823
Left Amygdala	0.240	0.735	0.531	0.968	0.066	0.197	0.722	0.897
Left Accumbens	0.523	0.818	0.874	0.968	**0.040**	0.197	0.691	0.897
Right Cerebral White Matter	0.415	0.735	0.691	0.968	0.125	0.327	0.806	0.930
Right Cerebral Cortex	0.139	0.735	0.654	0.968	**0.009**	0.197	0.549	0.823
Right Lateral Ventricle	0.412	0.735	0.089	0.930	0.484	0.598	**0.044**	0.823
Right Thalamus	0.545	0.818	0.921	0.968	0.438	0.598	0.726	0.897
Right Caudate	0.161	0.735	0.894	0.968	0.303	0.530	0.422	0.823
Right Putamen	0.591	0.827	0.159	0.968	0.236	0.450	0.315	0.823
Right Pallidum	**0.048**	0.735	0.400	0.968	0.460	0.598	0.455	0.823
Right Hippocampus	0.691	0.832	0.943	0.968	0.429	0.598	0.493	0.823
Right Amygdala	0.654	0.832	0.068	0.930	0.885	0.941	0.421	0.823
Right Accumbens	0.281	0.735	0.270	0.968	0.941	0.941	0.254	0.823

Table A-5: Uncorrected and corrected *p*-value of each region from the Atlas 1 anatomical region-level analysis using SpCent to characterize BOLD signal

	Graz		LUMC-SCI		LUMC-MCI		LUMC-AD	
Atlas1 Region	P-val	FDR	P-val	FDR	P-Val	FDR	P-Val	FDR
Frontal Pole	0.598	0.971	0.183	0.484	0.427	0.932	0.753	0.861
Insular Cortex	0.524	0.971	0.198	0.484	0.542	0.932	0.694	0.854
Superior Frontal Gyrus	**0.020**	0.372	0.284	0.484	0.721	0.932	0.734	0.860
Middle Frontal Gyrus	0.662	0.971	0.343	0.484	0.457	0.932	0.821	0.880
Inferior Frontal Gyrus, pars triangularis	0.851	0.971	0.297	0.484	0.814	0.932	0.717	0.860
Inferior Frontal Gyrus, pars opercularis	0.891	0.971	0.313	0.484	0.799	0.932	0.578	0.804
Precentral Gyrus	0.587	0.971	0.335	0.484	0.835	0.932	**0.038**	0.432
Temporal Pole	0.915	0.971	0.180	0.484	0.528	0.932	0.597	0.804
Superior Temporal Gyrus, anterior division	0.462	0.971	0.542	0.620	0.678	0.932	0.160	0.606
Superior Temporal Gyrus, posterior division	0.479	0.971	0.074	0.484	0.511	0.932	0.204	0.608
Middle Temporal Gyrus, anterior division	0.928	0.971	0.723	0.755	0.096	0.932	0.324	0.648
Middle Temporal Gyrus, posterior division	0.189	0.971	0.286	0.484	0.443	0.932	0.392	0.727
Middle Temporal Gyrus, temporooccipital part	0.302	0.971	0.210	0.484	0.678	0.932	0.495	0.761
Inferior Temporal Gyrus, anterior division	0.179	0.971	**0.046**	0.484	0.400	0.932	0.958	0.958
Inferior Temporal Gyrus, posterior division	0.143	0.971	**0.044**	0.484	0.574	0.932	0.603	0.804
Inferior Temporal Gyrus, temporooccipital part	0.951	0.971	0.235	0.484	0.711	0.932	0.310	0.648
Postcentral Gyrus	0.109	0.873	0.333	0.484	0.727	0.932	**0.034**	0.432
Superior Parietal Lobule	0.485	0.971	0.586	0.654	0.370	0.932	0.215	0.608
Supramarginal Gyrus, anterior division	0.882	0.971	0.445	0.567	0.429	0.932	0.394	0.727
Supramarginal Gyrus, posterior division	0.766	0.971	0.168	0.484	0.553	0.932	0.503	0.761
Angular Gyrus	0.741	0.971	0.243	0.484	0.670	0.932	0.522	0.761
Lateral Occipital Cortex, superior division	0.245	0.971	0.194	0.484	0.707	0.932	0.169	0.606
Lateral Occipital Cortex, inferior division	**0.009**	0.372	0.814	0.831	0.273	0.932	0.113	0.582
Intracalcarine Cortex	0.837	0.971	0.074	0.484	0.366	0.932	0.430	0.761
Frontal Medial Cortex	0.782	0.971	0.449	0.567	0.871	0.950	0.245	0.614
Juxtapositional Lobule Cortex	0.489	0.971	0.496	0.595	0.354	0.932	0.314	0.648
Subcallosal Cortex	0.604	0.971	0.642	0.685	0.366	0.932	**0.005**	0.154
Paracingulate Gyrus	0.080	0.770	0.410	0.547	0.681	0.932	0.643	0.832
Cingulate Gyrus, anterior division	0.843	0.971	0.238	0.484	0.821	0.932	0.933	0.953
Cingulate Gyrus, posterior division	0.398	0.971	0.599	0.654	0.710	0.932	0.659	0.832
Precuneous Cortex	0.872	0.971	0.410	0.547	0.626	0.932	0.240	0.614
Cuneal Cortex	0.274	0.971	0.298	0.484	0.776	0.932	**0.049**	0.432
Frontal Orbital Cortex	0.840	0.971	0.099	0.484	0.798	0.932	0.513	0.761
Parahippocampal Gyrus, anterior division	0.692	0.971	0.952	0.952	0.823	0.932	0.819	0.880
Parahippocampal Gyrus, posterior division	0.440	0.971	0.481	0.592	0.971	0.971	0.160	0.606
Lingual Gyrus	0.528	0.971	0.210	0.484	0.946	0.971	0.101	0.582
Temporal Fusiform Cortex, anterior division	0.524	0.971	0.248	0.484	0.795	0.932	0.825	0.880
Temporal Fusiform Cortex, posterior division	0.832	0.971	0.097	0.484	0.424	0.932	**0.006**	0.154
Temporal Occipital Fusiform Cortex	0.216	0.971	0.164	0.484	0.775	0.932	0.054	0.432
Occipital Fusiform Gyrus	**0.027**	0.372	0.332	0.484	0.591	0.932	0.121	0.582
Frontal Opercular Cortex	0.949	0.971	0.134	0.484	0.968	0.971	0.865	0.903
Central Opercular Cortex	0.828	0.971	0.514	0.601	0.419	0.932	0.271	0.618
Parietal Opercular Cortex	0.628	0.971	0.237	0.484	0.230	0.932	0.177	0.606
Planum Polare	0.920	0.971	0.066	0.484	0.961	0.971	0.523	0.761
Heschl's Gyrus (includes H1 and H2)	0.512	0.971	0.146	0.484	0.519	0.932	0.503	0.761
Planum Temporale	0.971	0.971	0.325	0.484	0.761	0.932	0.256	0.614
Supracalcarine Cortex	0.860	0.971	0.093	0.484	0.451	0.932	0.210	0.608
Occipital Pole	**0.031**	0.372	0.090	0.484	0.518	0.932	0.103	0.582

Table A-6: Uncorrected and corrected *p*-value of each region from the Atlas 2 anatomical region-level analysis using SpCent to characterize BOLD signal

	Graz		SCI		MCI		AD	
Atlas2 Regions	P-val	FDR	P-val	FDR	P-Val	FDR	P-Val	FDR
Left Cerebral White Matter	0.432	0.996	0.067	0.338	0.180	0.995	0.349	0.957
Left Cerebral Cortex	0.885	0.996	0.180	0.391	0.591	0.995	0.255	0.957
Left Lateral Ventricle	0.952	0.996	0.078	0.338	0.098	0.995	0.879	0.991
Left Thalamus	0.683	0.996	0.134	0.391	0.304	0.995	0.247	0.957
Left Caudate	0.597	0.996	0.475	0.554	0.214	0.995	0.403	0.957
Left Putamen	0.095	0.996	0.189	0.391	0.807	0.995	0.944	0.991
Left Pallidum	0.954	0.996	0.438	0.541	0.530	0.995	0.944	0.991
Brain-Stem	0.387	0.996	0.917	0.952	0.717	0.995	0.501	0.957
Left Hippocampus	0.916	0.996	0.952	0.952	0.558	0.995	0.472	0.957
Left Amygdala	0.845	0.996	0.080	0.338	0.655	0.995	0.992	0.992
Left Accumbens	0.820	0.996	0.158	0.391	0.061	0.995	0.763	0.991
Right Cerebral White Matter	0.430	0.996	0.410	0.538	0.894	0.995	0.417	0.957
Right Cerebral Cortex	0.598	0.996	0.182	0.391	0.974	0.995	0.137	0.957
Right Lateral Ventricle	0.952	0.996	0.328	0.492	0.810	0.995	0.741	0.991
Right Thalamus	0.328	0.996	0.385	0.538	0.682	0.995	0.610	0.991
Right Caudate	0.996	0.996	0.319	0.492	0.995	0.995	0.399	0.957
Right Putamen	0.214	0.996	0.056	0.338	0.709	0.995	0.721	0.991
Right Pallidum	0.940	0.996	0.052	0.338	0.845	0.995	0.243	0.957
Right Hippocampus	0.728	0.996	0.712	0.787	0.369	0.995	0.865	0.991
Right Amygdala	0.051	0.996	0.205	0.391	0.547	0.995	0.325	0.957
Right Accumbens	0.283	0.996	0.295	0.492	0.932	0.995	0.843	0.991

Table A-7: Uncorrected and corrected *p*-value of each region from the Atlas 1 anatomical region-level analysis using SpVar to characterize BOLD signal

	Graz		LUMC-SCI		LUMC-MCI		LUMC-AD	
Atlas1 Region	P-val	FDR	P-val	FDR	P-Val	FDR	P-Val	FDR
Frontal Pole	0.664	0.900	0.917	0.917	0.963	0.994	0.378	0.977
Insular Cortex	0.782	0.923	**0.015**	0.422	0.898	0.994	0.909	0.989
Superior Frontal Gyrus	0.923	0.923	0.759	0.867	0.309	0.994	0.606	0.977
Middle Frontal Gyrus	0.826	0.923	0.240	0.502	0.712	0.994	0.399	0.977
Inferior Frontal Gyrus, pars triangularis	0.560	0.900	0.199	0.435	0.590	0.994	0.853	0.977
Inferior Frontal Gyrus, pars opercularis	0.471	0.900	0.305	0.562	0.758	0.994	0.875	0.977
Precentral Gyrus	0.513	0.900	0.139	0.422	0.878	0.994	0.461	0.977
Temporal Pole	0.839	0.923	**0.048**	0.422	0.526	0.994	0.989	0.989
Superior Temporal Gyrus, anterior division	0.490	0.900	0.326	0.563	0.673	0.994	0.611	0.977
Superior Temporal Gyrus, posterior division	0.599	0.900	0.101	0.422	0.674	0.994	0.852	0.977
Middle Temporal Gyrus, anterior division	0.390	0.900	0.115	0.422	0.731	0.994	0.932	0.989
Middle Temporal Gyrus, posterior division	0.068	0.752	0.088	0.422	0.949	0.994	**0.044**	0.701
Middle Temporal Gyrus, temporooccipital part	0.635	0.900	0.367	0.587	0.706	0.994	0.256	0.977
Inferior Temporal Gyrus, anterior division	**0.029**	0.752	0.263	0.523	0.192	0.994	0.738	0.977
Inferior Temporal Gyrus, posterior division	0.388	0.900	0.168	0.422	0.715	0.994	0.102	0.977
Inferior Temporal Gyrus, temporooccipital part	0.270	0.900	0.340	0.563	0.812	0.994	**0.014**	0.672
Postcentral Gyrus	0.662	0.900	0.160	0.422	0.474	0.994	0.179	0.977
Superior Parietal Lobule	0.876	0.923	0.857	0.894	0.499	0.994	0.411	0.977
Supramarginal Gyrus, anterior division	0.589	0.900	0.436	0.633	0.962	0.994	0.871	0.977
Supramarginal Gyrus, posterior division	0.581	0.900	0.708	0.849	0.389	0.994	0.740	0.977
Angular Gyrus	0.806	0.923	0.817	0.894	0.712	0.994	0.801	0.977
Lateral Occipital Cortex, superior division	0.252	0.900	0.524	0.719	0.511	0.994	0.345	0.977
Lateral Occipital Cortex, inferior division	0.910	0.923	0.856	0.894	**0.023**	0.994	0.608	0.977
Intracalcarine Cortex	0.675	0.900	0.273	0.523	0.315	0.994	0.853	0.977
Frontal Medial Cortex	0.590	0.900	0.878	0.897	0.651	0.994	0.550	0.977
Juxtapositional Lobule Cortex	0.616	0.900	0.557	0.743	0.516	0.994	0.741	0.977
Subcallosal Cortex	0.527	0.900	0.399	0.598	0.962	0.994	0.660	0.977
Paracingulate Gyrus	0.375	0.900	0.199	0.435	0.977	0.994	0.648	0.977
Cingulate Gyrus, anterior division	0.078	0.752	0.110	0.422	0.914	0.994	0.604	0.977
Cingulate Gyrus, posterior division	0.601	0.900	0.614	0.797	0.752	0.994	0.954	0.989
Precuneous Cortex	0.579	0.900	0.730	0.855	0.622	0.994	0.799	0.977
Cuneal Cortex	0.471	0.900	0.089	0.422	0.140	0.994	0.853	0.977
Frontal Orbital Cortex	0.911	0.923	0.176	0.422	0.798	0.994	0.419	0.977
Parahippocampal Gyrus, anterior division	0.056	0.752	0.645	0.814	0.833	0.994	0.409	0.977
Parahippocampal Gyrus, posterior division	0.200	0.900	0.853	0.894	0.476	0.994	**0.036**	0.701
Lingual Gyrus	0.661	0.900	0.329	0.563	0.263	0.994	0.276	0.977
Temporal Fusiform Cortex, anterior division	0.506	0.900	0.524	0.719	0.242	0.994	0.282	0.977
Temporal Fusiform Cortex, posterior division	0.061	0.752	0.169	0.422	0.085	0.994	0.742	0.977
Temporal Occipital Fusiform Cortex	0.556	0.900	0.399	0.598	0.429	0.994	0.868	0.977
Occipital Fusiform Gyrus	0.361	0.900	0.687	0.846	**0.044**	0.994	0.564	0.977
Frontal Opercular Cortex	0.477	0.900	0.091	0.422	0.994	0.994	0.811	0.977
Central Opercular Cortex	0.887	0.923	**0.038**	0.422	0.747	0.994	0.446	0.977
Parietal Opercular Cortex	0.760	0.923	0.118	0.422	0.913	0.994	0.398	0.977
Planum Polare	0.906	0.923	0.103	0.422	0.978	0.994	0.429	0.977
Heschl's Gyrus (includes H1 and H2)	0.512	0.900	**0.039**	0.422	0.916	0.994	0.649	0.977
Planum Temporale	0.303	0.900	0.090	0.422	0.835	0.994	0.971	0.989
Supracalcarine Cortex	0.276	0.900	0.170	0.422	0.164	0.994	0.555	0.977
Occipital Pole	0.881	0.923	0.156	0.422	0.344	0.994	0.561	0.977

Table A-8: Uncorrected and corrected *p*-value of each region from the Atlas 2 anatomical region-level analysis using SpVar to characterize BOLD signal

	Graz		SCI		MCI		AD	
Atlas2 Regions	P-val	FDR	P-val	FDR	P-Val	FDR	P-Val	FDR
Left Cerebral White Matter	0.811	0.976	0.362	0.885	0.765	0.960	0.141	0.900
Left Cerebral Cortex	0.709	0.976	0.143	0.885	0.850	0.960	0.542	0.900
Left Lateral Ventricle	0.196	0.976	0.258	0.885	0.753	0.960	0.538	0.900
Left Thalamus	0.976	0.976	0.396	0.885	0.852	0.960	0.229	0.900
Left Caudate	0.874	0.976	0.610	0.900	0.584	0.960	0.589	0.900
Left Putamen	0.352	0.976	0.392	0.885	0.322	0.960	0.167	0.900
Left Pallidum	0.795	0.976	0.439	0.885	0.206	0.863	0.556	0.900
Brain-Stem	0.664	0.976	0.523	0.885	0.989	0.989	0.723	0.952
Left Hippocampus	0.762	0.976	0.876	0.931	0.318	0.960	0.875	0.959
Left Amygdala	0.052	0.565	0.052	0.885	0.828	0.960	0.600	0.900
Left Accumbens	0.632	0.976	0.906	0.931	0.799	0.960	0.258	0.900
Right Cerebral White Matter	0.946	0.976	0.695	0.900	0.868	0.960	0.304	0.900
Right Cerebral Cortex	0.917	0.976	0.535	0.885	0.593	0.960	0.882	0.959
Right Lateral Ventricle	0.081	0.565	0.548	0.885	0.760	0.960	0.226	0.900
Right Thalamus	0.605	0.976	0.931	0.931	0.476	0.960	0.580	0.900
Right Caudate	0.670	0.976	0.728	0.900	0.099	0.863	0.848	0.959
Right Putamen	0.079	0.565	0.318	0.885	0.148	0.863	0.400	0.900
Right Pallidum	0.243	0.976	0.345	0.885	0.923	0.969	0.990	0.990
Right Hippocampus	0.800	0.976	0.654	0.900	0.168	0.863	0.725	0.952
Right Amygdala	0.771	0.976	0.144	0.885	0.072	0.863	0.914	0.959
Right Accumbens	0.391	0.976	0.877	0.931	0.844	0.960	0.492	0.900

Table A-9: Uncorrected and corrected *p*-value of each region from the Atlas 1 anatomical region-level analysis using SpSkew to characterize BOLD signal

	Graz		LUMC-SCI		LUMC-MCI		LUMC-AD	
Atlas1 Region	P-val	FDR	P-val	FDR	P-Val	FDR	P-Val	FDR
Frontal Pole	0.160	0.859	0.201	0.321	0.696	0.997	0.638	0.729
Insular Cortex	0.543	0.991	0.179	0.306	0.506	0.997	0.256	0.473
Superior Frontal Gyrus	**0.011**	0.387	0.291	0.388	0.943	0.997	0.365	0.547
Middle Frontal Gyrus	0.173	0.859	0.219	0.340	0.476	0.997	0.616	0.721
Inferior Frontal Gyrus, pars triangularis	0.534	0.991	0.339	0.428	0.997	0.997	0.177	0.389
Inferior Frontal Gyrus, pars opercularis	0.415	0.991	0.243	0.363	0.944	0.997	0.874	0.893
Precentral Gyrus	0.561	0.991	0.156	0.277	0.767	0.997	**0.005**	0.106
Temporal Pole	0.857	0.991	0.069	0.277	0.688	0.997	0.520	0.675
Superior Temporal Gyrus, anterior division	0.874	0.991	0.185	0.307	0.764	0.997	0.122	0.370
Superior Temporal Gyrus, posterior division	0.640	0.991	**0.039**	0.277	0.891	0.997	0.071	0.298
Middle Temporal Gyrus, anterior division	0.590	0.991	0.435	0.475	**0.023**	0.997	0.426	0.601
Middle Temporal Gyrus, posterior division	0.234	0.859	0.116	0.277	0.318	0.997	0.734	0.801
Middle Temporal Gyrus, temporooccipital part	0.320	0.937	0.137	0.277	0.971	0.997	0.520	0.675
Inferior Temporal Gyrus, anterior division	0.311	0.937	**0.029**	0.277	0.352	0.997	0.874	0.893
Inferior Temporal Gyrus, posterior division	0.070	0.582	**0.012**	0.277	0.979	0.997	0.855	0.893
Inferior Temporal Gyrus, temporooccipital part	0.521	0.991	0.122	0.277	0.730	0.997	0.578	0.694
Postcentral Gyrus	0.138	0.859	0.105	0.277	0.522	0.997	**0.007**	0.106
Superior Parietal Lobule	0.742	0.991	0.478	0.510	0.153	0.997	0.107	0.366
Supramarginal Gyrus, anterior division	0.928	0.991	0.249	0.363	0.132	0.997	0.326	0.539
Supramarginal Gyrus, posterior division	0.585	0.991	0.055	0.277	0.744	0.997	0.278	0.493
Angular Gyrus	0.602	0.991	0.128	0.277	0.937	0.997	0.560	0.690
Lateral Occipital Cortex, superior division	0.377	0.991	0.115	0.277	0.932	0.997	0.178	0.389
Lateral Occipital Cortex, inferior division	**0.024**	0.387	0.381	0.446	0.190	0.997	**0.025**	0.199
Intracalcarine Cortex	0.968	0.997	0.051	0.277	0.821	0.997	0.235	0.450
Frontal Medial Cortex	0.478	0.991	0.608	0.621	0.898	0.997	0.363	0.547
Juxtapositional Lobule Cortex	0.732	0.991	0.288	0.388	0.376	0.997	0.137	0.370
Subcallosal Cortex	0.899	0.991	0.374	0.446	0.610	0.997	**0.012**	0.134
Paracingulate Gyrus	**0.023**	0.387	0.573	0.598	0.766	0.997	0.364	0.547
Cingulate Gyrus, anterior division	0.929	0.991	0.430	0.475	0.754	0.997	0.384	0.558
Cingulate Gyrus, posterior division	0.197	0.859	0.428	0.475	0.757	0.997	0.452	0.620
Precuneous Cortex	0.708	0.991	0.359	0.442	0.922	0.997	0.300	0.514
Cuneal Cortex	0.232	0.859	0.088	0.277	0.676	0.997	**0.032**	0.199
Frontal Orbital Cortex	0.895	0.991	0.106	0.277	0.611	0.997	0.067	0.298
Parahippocampal Gyrus, anterior division	0.818	0.991	0.731	0.731	0.569	0.997	0.994	0.994
Parahippocampal Gyrus, posterior division	0.251	0.859	0.272	0.384	0.802	0.997	0.140	0.370
Lingual Gyrus	0.673	0.991	0.091	0.277	0.997	0.997	**0.033**	0.199
Temporal Fusiform Cortex, anterior division	0.752	0.991	0.137	0.277	0.558	0.997	0.718	0.801
Temporal Fusiform Cortex, posterior division	0.882	0.991	0.077	0.277	0.285	0.997	**0.003**	0.106
Temporal Occipital Fusiform Cortex	0.237	0.859	0.083	0.277	0.578	0.997	**0.014**	0.134
Occipital Fusiform Gyrus	0.064	0.582	0.123	0.277	0.357	0.997	0.154	0.370
Frontal Opercular Cortex	0.984	0.997	0.151	0.277	0.781	0.997	0.535	0.675
Central Opercular Cortex	0.997	0.997	0.323	0.419	0.403	0.997	0.124	0.370
Parietal Opercular Cortex	0.781	0.991	0.090	0.277	0.269	0.997	0.081	0.298
Planum Polare	0.756	0.991	**0.047**	0.277	0.813	0.997	0.232	0.450
Heschl's Gyrus (includes H1 and H2)	0.332	0.937	0.146	0.277	0.416	0.997	0.202	0.421
Planum Temporale	0.784	0.991	0.143	0.277	0.800	0.997	0.154	0.370
Supracalcarine Cortex	0.871	0.991	**0.043**	0.277	0.937	0.997	0.078	0.298
Occipital Pole	0.073	0.582	**0.040**	0.277	0.963	0.997	0.056	0.298

Table A-10: Uncorrected and corrected *p*-value of each region from the Atlas 2 anatomical region-level analysis using SpSkew to characterize BOLD signal

	Graz		SCI		MCI		AD	
Atlas2 Regions	P-val	FDR	P-val	FDR	P-Val	FDR	P-Val	FDR
Left Cerebral White Matter	0.545	0.966	**0.036**	0.258	0.288	0.935	0.236	0.917
Left Cerebral Cortex	0.834	0.966	0.086	0.258	0.677	0.935	0.113	0.917
Left Lateral Ventricle	0.813	0.966	**0.025**	0.258	**0.020**	0.412	0.380	0.917
Left Thalamus	0.861	0.966	0.132	0.307	0.728	0.935	0.560	0.917
Left Caudate	0.587	0.966	0.681	0.753	0.393	0.935	0.733	0.917
Left Putamen	0.377	0.966	0.254	0.445	0.871	0.935	0.917	0.917
Left Pallidum	0.711	0.966	0.483	0.614	0.358	0.935	0.827	0.917
Brain-Stem	0.744	0.966	0.790	0.830	0.857	0.935	0.482	0.917
Left Hippocampus	0.842	0.966	0.889	0.889	0.639	0.935	0.289	0.917
Left Amygdala	0.867	0.966	0.077	0.258	0.605	0.935	0.877	0.917
Left Accumbens	0.874	0.966	0.604	0.705	0.070	0.735	0.260	0.917
Right Cerebral White Matter	0.652	0.966	0.219	0.445	0.819	0.935	0.244	0.917
Right Cerebral Cortex	0.694	0.966	0.082	0.258	0.890	0.935	**0.044**	0.915
Right Lateral Ventricle	0.779	0.966	0.233	0.445	0.940	0.940	0.852	0.917
Right Thalamus	0.297	0.966	0.400	0.600	0.417	0.935	0.673	0.917
Right Caudate	0.857	0.966	0.371	0.599	0.846	0.935	0.565	0.917
Right Putamen	0.270	0.966	**0.047**	0.258	0.858	0.935	0.744	0.917
Right Pallidum	0.985	0.985	0.054	0.258	0.682	0.935	0.437	0.917
Right Hippocampus	0.941	0.985	0.489	0.614	0.747	0.935	0.707	0.917
Right Amygdala	**0.044**	0.932	0.106	0.277	0.545	0.935	0.573	0.917
Right Accumbens	0.507	0.966	0.497	0.614	0.410	0.935	0.695	0.917

Appendix B: Multivariate: Hotelling's two-sample *t*-squared statistic

Hotelling's two-sample t^2 statistic is used for multivariate statistical hypothesis testing (Hotelling, 1931). This test statistic allows for comparison of two or more statistical measures. In our context, we can compare multiple statistical measure of the fMRI signal, such as the standard deviation and ALFF, and test if they are statistically different between the two populations. Using more covariates can lead to an increase in precision in differentiating different populations. It uses the joint probability distribution of the various statistical measures used. The statistic is defined as:

$$t^2 = \frac{n_1 n_2}{n_1 + n_2} (\overline{X_1} - \overline{X_2})^{\mathrm{T}} \hat{\mathbf{\Sigma}}^{-1} (\overline{X_1} - \overline{X_2}) \tag{14}$$

using the unbiased pooled covariance matrix estimate:

$$\hat{\mathbf{\Sigma}} = \frac{(n_1 - 1)\hat{\mathbf{\Sigma}}_1 + (n_2 - 1)\hat{\mathbf{\Sigma}}_2}{n_1 + n_2 - 2} \tag{15}$$

where $\hat{\mathbf{\Sigma}}_i = \frac{1}{(n_i - 1)} \sum_{j=1}^{n_i} (X_{ij} - \overline{X_i})(X_{ij} - \overline{X_i})^{\mathrm{T}}$ is the sample covariance matrix of population i.

Hotelling's two-sample *t*-squared statistic is usually compared to the F-distribution using the following relation:

$$F = \frac{n_1 + n_2 - p - 1}{(n_1 + n_2 - 2)p} \cdot t^2 \tag{16}$$

where p is the number of statistical measures used.

However, in line with thesis, permutation testing can also be used to generate the null probability to minimise any assumptions required for the F-distribution.